

---

# HAQT deliverable 3-3: AQ instrument benchmarking report in the laboratory and in the field

---

Petäjä, T.<sup>1</sup>, Paasonen, P.<sup>1</sup>, Häkkinen, E.<sup>1</sup>, Vainio, T.<sup>1</sup>, Shahriyer, A.<sup>1</sup>, Lusa, K.<sup>2</sup>, Saarnio, K.<sup>2</sup>, Waldén, J.<sup>2</sup>, Mäkelä, T.<sup>3</sup>, Julkunen, A.<sup>3</sup>, Kuula, J.<sup>2</sup>, Niemi, J.V.<sup>3</sup>, Saukko, E.<sup>4</sup>, Järvinen, A.<sup>5</sup> and Timonen, H.<sup>2</sup> and the HAQT project team

<sup>1</sup>Institute of Atmospheric and Earth System Science / Physics, Faculty of Science, University of Helsinki, Finland

<sup>2</sup>Finnish Meteorological Institute, Helsinki, Finland

<sup>3</sup>Helsinki Region Environmental Services Authority (HSY), Finland

<sup>4</sup>Pegasor Oy, Tampere, Finland

<sup>5</sup>Vaisala Oyj, Vantaa, Finland

15/08/2019

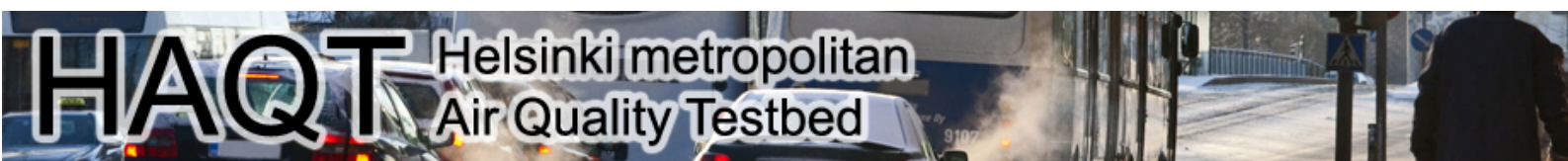


## Table of Contents

Table of Contents.....	1
1. Introduction .....	2
2. Description of the sensors .....	2
2.1 Vaisala AQT 420 (2017 Release).....	2
2.2 Pegasor AQ Urban instrument.....	3
3. Laboratory verification, results and discussion .....	3
3.1.1 Protocol and requirements for gas sensor performance testing .....	3
3.1.2 Laboratory test setup.....	4
3.1.3 Test results in prevailing room conditions .....	7
3.1.4 Test results in the exposure chamber .....	8
3.2 Aerosol measurements.....	12
4. Atmospheric measurements .....	15
4.1 Side-by-side intercomparison against the reference method and performance against AQ-directive.....	15
4.2 Correction factors for the AQT 420 sensors (2017 Release).....	19
4.2.1 NO <sub>2</sub> concentrations.....	21
4.2.2 CO concentrations .....	24
4.2.3 Ozone.....	29
4.2.4 PM10.....	33
4.2.4.1 PM10 and RH.....	37
4.2.5 Relative humidity and temperature .....	38
4.3 Precision and accuracy of the Pegasor AQ Urban.....	39
5. Conclusions.....	41
5.1 Laboratory results .....	41
5.2 Atmospheric observations.....	41
References.....	43

## 1. Introduction

Air quality is governed by both gas-phase components, such as ozone ( $O_3$ ), nitrogen oxides ( $NO_x$ ), and aerosol particles (mass and number concentration). There is a substantial variability within the city in the particulate and gas phase pollutant concentrations (e.g. von Bismarck-Osten et al. 2013, Zhao et al. 2018). This variability leads to uncertainties of personal exposure estimates for the urban dwellers (e.g. Park and Kwan, 2017).

Due to this heterogeneity, the observations need to be performed in a network of air quality stations, which need to be supplemented with additional cost-effective instruments (e.g. de Nazelle et al. 2013) in combination with detailed air quality modelling (Kukkonen et al. 2016). With a such combination is required for a comprehensive understanding of the current air quality situation and its spatio-temporal variation, health effects and personal exposure (Morawska et al. 2018). The HAQT tackles this issue by combining measurement network consists of three different types of AQ instruments: reference-level instruments of the HSY network and a suite of commercial, more affordable instruments from Vaisala (AQT 420, 2017 Release), and Pegasor in a combination of ENFUSER modeling platform (Johansson et al. 2015).

As a part of the HAQT workpackage (WP) 3, we evaluated the performance level of the new, cost-effective AQ instruments. We performed a combination of detailed laboratory experiments and long-term atmospheric observations. These tests were carried out both in a controlled laboratory environment and in field conditions. These activities include both trace gas measurements and aerosol mass measurements.

The aim of this report is to summarize the work performed in the laboratory and in the field in a single report as a deliverable 3.3 for the HAQT project. We report the performance of AQT 420 (2017 Release) sensors for both trace gas concentrations and aerosol mass measurements as well as report on side-by-side intercomparison activities of the AQT 420 and Pegasor sensors against the reference instrumentation in ambient conditions.

## 2. Description of the sensors

### 2.1 Vaisala AQT 420 (2017 Release)

The Vaisala Air Quality Transmitter AQT 420 (Release 2017), from now on AQT 420, combines electrochemical methods and optical aerosol counting. The former provides ppb level observation capacity of common gas phase pollutants, such as nitrogen oxides dioxide ( $NO_x$ ), sulphur dioxide ( $SO_2$ ), carbon monoxide (CO) and ozone ( $O_3$ ) and the latter provide a measure of aerosol mass concentration. The instrument is complemented with ancillary meteorological observations (Vaisala, 2019). The Vaisala AQT 420 sensor package enables cost-effective observations of air quality parameters in a dense observation network.

The aerosol particles are detected with a laser particle counter, which is based on scattering of light. The measurements are converted to aerosol mass in PM<sub>2.5</sub> and PM<sub>10</sub> mass categories assuming a constant density. At relatively large input number concentrations the diameter measurement range is between 0.3 and 10  $\mu m$  (spherical equivalent). The detection efficiency is dependent on aerosol concentration. With a small input number concentration, the smallest detectable particle size is larger as the detection relies on the extinction caused by the sample population as a whole. The mass concentration range is from 0 to 2000  $\mu g m^{-3}$  with PM<sub>2.5</sub> and from 0 to 5000  $\mu g m^{-3}$  with PM<sub>10</sub>, with measurement resolution of 0.1  $\mu g m^{-3}$ .

## 2.2 Pegasor AQ Urban instrument

Pegasor AQ Urban is a diffusion charging-based particulate matter instrument which measures lung deposited surface area (LDSA) of aerosol particles. The measurement principle is as follows: a unipolar corona charger forms cluster ions, which are driven onto the surfaces of the particles by diffusional forces. Subsequently the current collected onto an electrometer is measured. The current (i.e. number of ions) is proportional to the surface area that corresponds to lung deposited surface area of the particles. Current signal is measured at the outlet of the device using a so-called measurement of escaping current. This measurement technique is specifically applicable to the measurements of small particles (diameter < 400 nm), which are typically emitted from local combustion sources such as vehicular and residential wood burning emissions (Kuula et al., 2018).

The sampling to the instrument is drawn from a weather protected, high turnover air inlet enclosure, protected from rainwater, snow, insects and coarse matter ingress. The sample is heated to +40°C above ambient temperature to evaporate water from the particles and prevent fog droplets from entering the sensor. The sensitivity with respect to LDSA is  $0.215 \mu\text{m cm}^{-2} \text{fA}^{-1}$ , with sensitivity of the electrometer being in the low fA range at 1 Hz data acquisition. With longer integration times, better sensitivity can be achieved. The nominal integration time is 2 min, but it can be adjusted freely. The response characteristics of the AQ Urban has been previously described in Rostedt et al. 2014 and Järvinen et al. 2015.

In the HAQT project, all Pegasor AQ Urban instruments were updated at the beginning June 2018 (PPS-M4 measurement units with firmware version 1.14, 31.5.2018).

## 3. Laboratory verification, results and discussion

### 3.1 Trace gases

#### ***3.1.1 Protocol and requirements for gas sensor performance testing***

The performance of the Vaisala Air Quality Transmitter AQT420 sensor systems were tested in laboratory conditions against reference methods following the draft document that was being developed and constantly updated by the CEN/TC264/WG42: "Air quality – Performance evaluation of air quality sensors – Part 1: Gaseous pollutants in ambient air". The aim of the test program was to evaluate, if the performance of the selected type of instruments are applicable for air quality measurements fulfilling the data quality objective for indicative measurements according to Air Quality Directive 2008/50/EC. Based on the results of the performance characteristics of the instruments, the uncertainty budget for the measurement results was prepared.

The sensor testing protocol described in the above-mentioned CEN Technical Specification draft starts with pre-tests including the estimation of the time of response of the sensor (rise and fall time), lack of fit of the calibration function, the repeatability of measurements and limit of detection. The following tests are to be performed for the extended evaluation of sensors in laboratory or at field sites according to the latest version of the draft document: short and long term drifts, cross sensitivities by gaseous interfering compounds, humidity effect, temperature effect, memory effect of sensor for the main pollutant, and memory effect when changing the level of temperature and humidity.

The response time of sensors is estimated by the time needed for the sensor to reach 90 % of the final stable value after a change of test gas level from zero to span (rise time) and from span to zero (fall time). The change of gas concentration shall be made as fast as possible. Lack of fit test is made as a multipoint calibration (4 concentration levels including zero and full scale). Measurements for the short-term drift are carried out at zero and span approximatively with about 24 hours intervals for 3 days.

The sensor performance requirements per type of test depend on the classification, in which the sensor is able to reach based on the test results (Class 1 has the highest requirements and Class 3 the lowest): For example, the requirement for Class 1 sensor systems is to have response time smaller than  $\frac{1}{2}$  of averaging time (generally 1 h) at traffic site or  $\frac{1}{3}$  of averaging time (generally 1 h) at background sites, whereas for Classes 2 and 3 it is required to have response time smaller than  $\frac{1}{4}$  of averaging time (generally 1 h) at background station. The standard uncertainty due to the lack of fit of a calibration function must be less than 8 % of upper assessment threshold in case of Class 1, and for Classes 2 and 3 it must be less than 12 % of lower assessment threshold; additionally, the slope and the intercept of calibration should not differ significantly from 1 and 0, respectively. The requirements for repeatability and limit of detection depend widely on the compound and performance class.

### ***3.1.2 Laboratory test setup***

The sensor tests were originally started in the Air Quality Calibration Laboratory of the Finnish Meteorological Institute in the prevailing room temperature and humidity; several evaluation tests were performed under these conditions.

Test gases were produced using methods included in the accredited quality system of the laboratory. Determinations of the test gas concentrations are made using reference measuring methods defined in EN method standards, i.e. chemiluminescence (NO, NO<sub>2</sub>), ultraviolet photometry (O<sub>3</sub>), ultraviolet fluorescence (SO<sub>2</sub>) and non-dispersive infrared absorption (CO). The used analysers were calibrated with SI-unit traceable standard gases.

One of the used methods to produce test gases was dynamic dilution, where SI-unit traceable high concentration reference gas standards (CO, SO<sub>2</sub>) were diluted by a mass flow controller-based device (EnviroNics 4000). Mass flow controllers automatically control the flow rate of a gas according to a set flow and they are calibrated against SI-traceable flow measurement standard.

Dynamic dilution was used to produce NO<sub>2</sub> test gas. In this case, the source of NO<sub>2</sub> was permeation tube, in which the gas has been pressed in liquid form. The tube is closed tightly in both ends, with the exception of a small area where the gas can permeate from the tube. When the tube is kept in constant conditions (temperature, pressure), the permeation rate of the gas from the liquefied form is constant.

Ozone test gases were produced by the ozone generator of Sonimix 6000-dilutor and determined by Dasibi 1008AH analyzer (SI-traceable photometer). The used zero air for all the dilutions is compressed and purified air.

There were three (and later on four) AQT420 sensor systems (2017 Release) under the performance testing in prevailing room conditions (referred here as Sensors no. 1, no. 2, no. 3 and no. 4). The sensor systems were of model of year 2017 (software version 1.14). The sensor units were connected to the Evidas Ultimate data acquisition system that was used for collecting the measured data. In these tests, all of the three or four sensor units were under evaluation at the same time. The flow of the test gas was divided equally to each sensor. Amount of the total flow varied depending of the gas

component and the concentration of the span gas. The gas flow was humidified to match with the prevailing room humidity. The gas flow humidifying system contained a circulating water bath and a Perma Pure Nafion tubing (Figure 3.1.1). Adjustment of the humidity of the testing gas was made manually by changing the ratio of the dry and humidified gas flow.

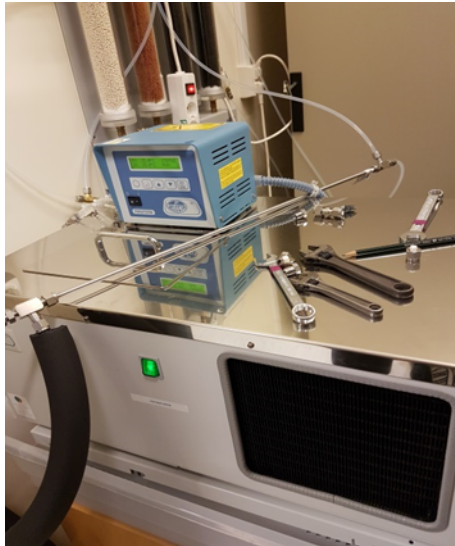


**Figure 3.1.1** Gas flow humidifying system.

In the second phase of the performance tests, the above-mentioned draft document for sensor performance evaluation was updated giving now requirement to perform the tests in an exposure chamber. Therefore, an exposure chamber was prepared for testing the gas sensors in controlled conditions (adjustable temperature and humidity). The shape of the exposure chamber is cylindrical with the inside length of 92 cm and the inner diameter of about 30 cm. The chamber is made of steel and its inner surfaces are coated with polytetrafluoro-ethylene (PTFE). Photos of the exposure chamber are presented in Figure 3.1.2.



**Figure 3.1.2** Example photos of the test chamber.

Temperature of the exposure chamber was adjusted using a refrigerated circulating liquid bath (LAUDA-Brinkmann ECO Silver, stainless steel), where the used liquid was a mixture of water and glycol (about 1:1). The water-glycol mixture circulates in a tubing around the chamber keeping the inside temperature of the chamber at a constant and required level. The required temperature for NO<sub>2</sub>, SO<sub>2</sub> and CO tests is 15±2 °C and for O<sub>3</sub> tests 22±2 °C. In addition, three other temperature levels are

needed to test temperature effects for the gas sensors (altogether 4 levels, between -20 °C and 40 °C, set for the range of field temperature).

The gas flow humidifying was made similarly as described above. In exposure chamber tests, the humidity conditions should be stable and constant during each test. Requirement for the humidity level is 50±5 %RH. In addition, three other humidity levels are needed to test humidity effects for the gas sensors (between 10 and 25 %, between 70 and 75 %, and 90 %).

Three sensor units were placed in a row in the exposure chamber. These were the same sensor units that were tested in the prevailing room conditions (Sensors no. 1, no. 2 and no. 4). However, before the commencement of tests in the exposure chamber, the sensor units had to be updated with a newer version of the software (version 2.08). Therefore, the results of the two separate performance tests cannot be compared directly with each other. The sensor units were connected to the Ultimate data acquisition system that was used for collecting the measured data. The flow of the test gas was divided equally to each sensor. Amount of the total flow varied depending of the gas component and the concentration of the span gas. For example, when testing the NO<sub>2</sub> sensors the flow level was 960 ml/min.

The sensor test protocol seemed to require a lot of time and therefore the progress in performance testing was slow. Additionally, there was not enough time to do tests with all the four gases and therefore NO<sub>2</sub> and O<sub>3</sub> were prioritized. Also temperature effects and cross sensitivities had to be left undone due to lack of time. Unluckily, one of the sensor units (no. 4) stopped working during the testing and due to lack of time, the tests had to be finished with two sensor units only.

After the chamber exposure tests, the two remaining sensor systems were installed at Mäkelänkatu traffic station for two months for an applied long term drift test. This applied protocol differs from the one presented in the draft of the Technical Specification: The sensors measured ambient air parallel to the reference methods maintained at the station (NO<sub>2</sub>: chemiluminescence; O<sub>3</sub>: UV-photometry). The results were averaged to daily values, and the results of sensors were compared to those of the reference methods. The long term drift (D<sub>LD</sub>) is estimated as the average of differences between two consecutive values (sensor–reference) with 15 days (day 1, 15, 30, 45 and 60) using equation 1:

$$D_{LD} = \frac{\sum_{i=1}^5 |C_{i,after} - C_{i,before}|}{4} \tag{1}$$

### 3.1.3 Test results in prevailing room conditions

The results of the pre-tests made in the prevailing laboratory room conditions are presented in Table 3.1.1 for NO<sub>2</sub>, in Table 3.1.2 for O<sub>3</sub>, in Table 3.1.3 for SO<sub>2</sub>, and in Table 3.1.4 for CO.

**Table 3.1.1** NO<sub>2</sub> sensor pre-test results in prevailing room conditions.

Test quantity	Sensor no. 1	Sensor no. 2	Sensor no. 3	unit
Response time, t <sub>90</sub> (rise)	27.3 ± 0.6	27.3 ± 0.6	25.0 ± 1.0	minute (average ± stdev)
Response time, t <sub>90</sub> (fall)	23.3 ± 0.6	23.3 ± 0.6	21.3 ± 0.6	minute (average ± stdev)
Response time, t <sub>90</sub>	24.7 ± 2.3	24.5 ± 2.7	23.0 ± 2.6	minute (average ± stdev)
Lack of fit of calibration function	7.8	6.7	5.9	maximum residual (%)
Regression	1.138y-9.025	1.093y-11.647	1.472y-1.251	coefficients
Repeatability	30.6	34.5	18.8	µg/m <sup>3</sup> (stdev in full scale)
Limit of detection	0.9	1.0	0.3	µg/m <sup>3</sup> (3x stdev in zero)

**Table 3.1.2** O<sub>3</sub> sensor pre-test results in prevailing room conditions.

Test quantity	Sensor no. 1	Sensor no. 2	Sensor no. 3	unit
Response time, t <sub>90</sub> (rise)	58.0 ± 27.9	67.3 ± 40.2	44.0 ± 12.8	minute (average ± stdev)
Response time, t <sub>90</sub> (fall)	21.7 ± 0.6	26.0 ± 1.7	20.7 ± 0.6	minute (average ± stdev)
Response time, t <sub>90</sub>	39.0 ± 24.7	32.0 ± 13.4	38.5 ± 26.0	minute (average ± stdev)
Lack of fit of calibration function	17.2	21.8	19.7	maximum residual (%)
Regression	1.527y+5.286	1.026y+7.202	1.143y+10.283	coefficients
Repeatability	20.6	23.7	42.9	µg/m <sup>3</sup> (stdev in full scale)
Limit of detection	0.2	0.2	1.2	µg/m <sup>3</sup> (3x stdev in zero)

**Table 3.1.3** SO<sub>2</sub> sensor pre-test results in prevailing room conditions.

Test quantity	Sensor no. 1	Sensor no. 2	Sensor no. 3	unit
Response time, t <sub>90</sub> (rise)	29.7 ± 0.6	25.3 ± 0.6	29.0 ± 1.0	minute (average ± stdev)
Response time, t <sub>90</sub> (fall)	27.0 ± 2.6	22.3 ± 2.3	26.0 ± 1.0	minute (average ± stdev)
Response time, t <sub>90</sub>	27.7 ± 2.7	23.3 ± 2.6	27.7 ± 3.1	minute (average ± stdev)
Lack of fit of calibration function	2.6	2.3	2.3	maximum residual (%)
Regression	1.115y-3.009	1.591y-2.175	1.123y-2.019	coefficients
Repeatability	25.4	17.7	18.8	µg/m <sup>3</sup> (stdev in full scale)
Limit of detection	4.0	6.2	2.3	µg/m <sup>3</sup> (3x stdev in zero)

**Table 3.1.4** CO sensor pre-test results in prevailing room conditions.

Test quantity	Sensor no. 1	Sensor no. 2	Sensor no. 3	unit
Response time, $t_{90}$ (rise)	23.7 ± 0.6	23.7 ± 0.6	23.7 ± 0.6	minute (average ± stdev)
Response time, $t_{90}$ (fall)	23.7 ± 0.6	24.0 ± 0.0	23.7 ± 0.6	minute (average ± stdev)
Response time, $t_{90}$	23.7 ± 0.5	23.8 ± 0.4	23.7 ± 0.5	minute (average ± stdev)
Lack of fit of calibration function	1.1	1.8	1.9	maximum residual (%)
Regression	1.309y+85.46	1.232y+203.4	1.311y+140.3	coefficients
Repeatability	169.0	269.6	94.2	µg/m <sup>3</sup> (stdev in full scale)
Limit of detection	63.7	51.7	54.0	µg/m <sup>3</sup> (3x stdev in zero)

### 3.1.4 Test results in the exposure chamber

Due to limited time available, the performance tests for sensor systems in the exposure chamber had to be reduced to the most essential ones and they were continued in the field conditions. The results of the pre-tests and test for short term drift in the exposure chamber as well as long term drift in the field testing are presented in Table 3.1.5 for NO<sub>2</sub> and in Table 3.1.6 for O<sub>3</sub>.

**Table 3.1.5** NO<sub>2</sub> sensor test results in the exposure chamber.

Test quantity	Sensor no. 1	Sensor no. 2	Sensor no. 4	unit
Response time, $t_{90}$ (rise)	27.0 ± 1.0	26.7 ± 1.5	32.3 ± 2.5	minute (average ± stdev)
Response time, $t_{90}$ (fall)	24.0 ± 0.0	23.7 ± 0.6	25.3 ± 0.6	minute (average ± stdev)
Response time, $t_{90}$	25.5 ± 1.8	25.2 ± 1.9	28.8 ± 4.2	minute (average ± stdev)
Lack of fit of calibration function	2.7	2.3	7.4	maximum residual (%)
Regression	1.256y-11.453	1.103y-1.999	1.94	coefficients
Repeatability	2.4	2.7	7.2	µg/m <sup>3</sup> (stdev in full scale)
Limit of detection	8.0	4.5	1.7	µg/m <sup>3</sup> (3x stdev in zero)
Short term drift	3.3	3.1	4.7	µg/m <sup>3</sup> (average)
Long term drift*	6.7	8.5	-	µg/m <sup>3</sup> (average)

\*Long term drift determined in the field testing.

**Table 3.1.6** O<sub>3</sub> sensor test results in the exposure chamber.

Test quantity	Sensor no. 1	Sensor no. 2	Sensor no. 4	unit
Response time, t <sub>90</sub> (rise)	25.3 ± 0.6	25.0 ± 0.0	-	minute (average ± stdev)
Response time, t <sub>90</sub> (fall)	24.3 ± 1.5	24.7 ± 0.6	-	minute (average ± stdev)
Response time, t <sub>90</sub>	24.8 ± 1.2	24.8 ± 0.4	-	minute (average ± stdev)
Lack of fit of calibration function	29.7	28.2	-	maximum residual (%)
Regression	1.059y+0.471	0.854y-6.027	-	coefficients
Repeatability	6.7	2.9	-	µg/m <sup>3</sup> (stdev in full scale)
Limit of detection	15.7	3.5	-	µg/m <sup>3</sup> (3x stdev in zero)
Short term drift	5.9	2.6	-	µg/m <sup>3</sup> (average)
Long term drift*	8.7	8.8	-	µg/m <sup>3</sup> (average)

\*Long term drift determined in the field testing.

The sensor test results per type of test compared to preliminary performance requirements of three assessment regimes of classification of sensor systems (Classes 1, 2 and 3) in the draft of the Technical Specification of gas sensor performance tests are presented in Table 3.1.7 for NO<sub>2</sub> and in Table 3.1.8 for O<sub>3</sub>.

**Table 3.1.7** NO<sub>2</sub> sensor test results per type of test compared to preliminary performance requirements of three assessment regimes of classification of sensor systems.

Performance parameter	Test result of sensor no. 1	Test result of sensor no. 2	Class 1 sensor systems	Class 2 sensor systems	Class 3 sensor systems
<b>Response time, <math>t_{90}</math></b>	25.5 ± 1.8	25.2 ± 1.9	< 1/10 of averaging time (1h) at traffic sites <b>or</b> < 1/3 of averaging time (1h) at background sites	< 1/4 of averaging time (1h) at background sites	< 1/4 of averaging time (1h) at background sites
<b>Calibration uncertainty, <math>U(\text{lof})^{**}</math></b>	5.5	2.2	< 3.2 µg/m <sup>3</sup>	< 3.2 µg/m <sup>3</sup>	< 3.2 µg/m <sup>3</sup>
<b>Repeatability, <math>r</math></b>	5.4	6.5	≤ 7.6 µg/m <sup>3</sup>	≤ 11.5 µg/m <sup>3</sup>	≤ 23 µg/m <sup>3</sup>
<b>Limit of detection, LOD</b>	3.5	2.6	≤ 19.1 µg/m <sup>3</sup>	≤ 28.7 µg/m <sup>3</sup>	≤ 28.7 µg/m <sup>3</sup>
<b>Slope of calibration, <math>b</math> - uncertainty of <math>b</math></b>	0.796 0.008	0.906 0.004	not significantly differ from 1: $ b-1  \leq 2 \cdot u(b)$	not significantly differ from 1: $ b-1  \leq 2 \cdot u(b)$	no requirements
<b>Intercept of cal., <math>a</math> - uncertainty of <math>a</math></b>	9.121 1.238	1.812 0.569	not significantly differ from 0: $ a  \leq 2 \cdot u(a)$	not significantly differ from 0: $ a  \leq 2 \cdot u(a)$	no requirements
<b>Short term drift, <math>u(D_{SD})</math></b>	3.3	3.1	included in the uncertainty of long term drift	included in the uncertainty of long term drift	
<b>Long term drift, <math>u(D_{LD})^{**}</math></b>	7.6	9.6	expanded total measurement uncertainty ≤ 50%*	expanded total measurement uncertainty ≤ 100%*	expanded total measurement uncertainty ≤ 200%*
<b>Humidity effect, <math>u(X_{RH})^{**}</math></b>	0.97	1.97			

\*Expanded total measurement uncertainty includes standard uncertainties of several performance parameters multiplied by a covering factor of 2.

\*\*Standard uncertainties to be included in the expanded total measurement uncertainty determined in this project.

**Table 3.1.8** O<sub>3</sub> sensor test results per type of test compared to preliminary performance requirements of three assessment regimes of classification of sensor systems.

Performance parameter	Test result of sensor no. 1	Test result of sensor no. 2	Class 1 sensor systems	Class 2 sensor systems	Class 3 sensor systems
<b>Response time, t<sub>90</sub></b>	24.8 ± 1.2 minutes	24.8 ± 0.4 minutes	< 1/10 of averaging time (1h) at traffic sites <b>or</b> < 1/3 of averaging time (1h) at background sites	< 1/4 of averaging time (1h) at background sites	< 1/4 of averaging time (1h) at background sites
<b>Calibration uncertainty, U(lof)**</b>	11.4	14.6	< 6.7 µg/m <sup>3</sup>	< 7.2 µg/m <sup>3</sup>	< 7.2 µg/m <sup>3</sup>
<b>Repeatability, r</b>	20.2	9.0	≤ 8.0 µg/m <sup>3</sup>	≤ 12 µg/m <sup>3</sup>	≤ 24 µg/m <sup>3</sup>
<b>Limit of detection, LOD</b>	7.9	1.7	≤ 20 µg/m <sup>3</sup>	≤ 30 µg/m <sup>3</sup>	≤ 30 µg/m <sup>3</sup>
<b>Slope of calibration, b - uncertainty of b, u(b)</b>	0.944 0.046	1.171 0.043	not significantly differ from 1:  b-1  ≤ 2.u(b)	not significantly differ from 1:  b-1  ≤ 2.u(b)	no requirements
<b>Intercept of cal., a - uncertainty of a, u(a)</b>	-0.444 4.623	7.060 4.337	not significantly differ from 0:  a  ≤ 2.u(a)	not significantly differ from 0:  a  ≤ 2.u(a)	no requirements
<b>Short term drift, u(D<sub>SD</sub>)</b>	6.1	3.1	included in the uncertainty of long term drift	included in the uncertainty of long term drift	
<b>Long term drift, u(D<sub>LD</sub>)**</b>	9.4	10.9	expanded total measurement uncertainty ≤ 50%*	expanded total measurement uncertainty ≤ 100%*	expanded total measurement uncertainty ≤ 200%*
<b>Humidity effect, u(X<sub>RH</sub>)**</b>	1.28	3.37			

\*Expanded total measurement uncertainty includes standard uncertainties of several performance parameters multiplied by a covering factor of 2.

\*\*Standard uncertainties to be included in the expanded total measurement uncertainty determined in this project.

As a summary, the AQT420 sensor system (2017 Release) passed part of the requirements for test quantities or performance parameters for Class 1, Class 2 or Class 3 sensor systems; however, not all the requirements set in the draft of the Technical Specification being developed for the performance testing of air quality sensors were met. For some gases and test quantities the parallel sensor systems showed very similar results between each other but in some cases the results of parallel sensor systems differed notably. The most notable requirement exceedances were determined for response times of all the gas components investigated. This is mostly due to the algorithms used for calculating the measurement results of the individual measurement sensors; probably, by improving the algorithms of the AQT420 sensor system it is likely to fit into the required response times and thus also other test quantity requirements. Unfortunately, due to lack of time and resources, not all the proposed test quantities could be determined, and consequently, the total measurement uncertainty also could not be calculated.

### 3.2 Aerosol measurements

The detection efficiency of the AQT 420 optical sensor was determined in the laboratory with a laboratory setup that is similar to Single Charged aerosol Reference (SCAR) described in Yllojanperä et al. 2010. Our version is presented in Häkkinen (2017). The schematic of the calibration setup is described in Figure 3.2.

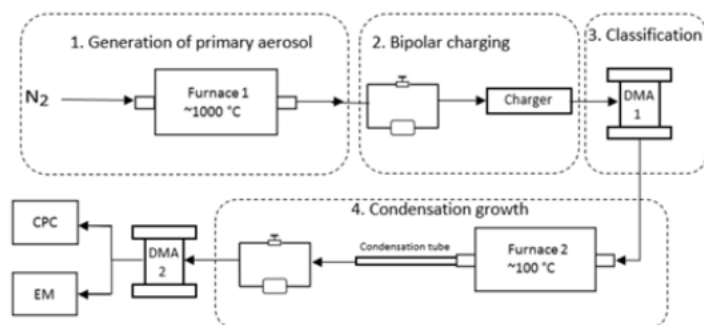


**Figure 3.2.1** Aerosol calibration setup SCAR used in this study.

The operation principle of the SCAR is the following: silver nanoparticles are generated in a furnace (Carbolite), where pure silver metal is heated to 1000 °C in pure nitrogen. As the flow cools down, silver vapor nucleates and forms silver nanoparticles in the size range of 5-50 nm. The particles are exposed to a large number of cluster ions produced with a radioactive source, which brings the aerosol population into a known charge distribution. The aerosol is directed to a Differential Mobility Analyzer (DMA, Winklmayr et al. 1991), which provides a narrow size of singly charged silver particles. In the next step, these particles are coated with organic surfactant. The second DMA selects again a narrow size distribution from these coated particles. These particles are in the size range from 100 nm to 1000 nm in electrical mobility equivalent diameter with only one elemental charge. These particles are directed to a Condensation Particle Counter (CPC, e.g. Mordas et al. 2008) that determines their number concentration and to AQT sensor. Detection efficiency measurements shown in Figure 3.2.3 where conducted with a large input number concentration. Thus, the AQT results demonstrate the sensor operation at cases where the primary measurement signal results from a population of particles instead of single particles.

In the first laboratory test, we tested the response of the AQT 420 sensor to a variable concentration of 500 nm aerosol particles. The CPC provided us the reference number concentration. The mass was calculated assuming size of 500 nm with the density of the organic surfactant (Diethylhexylsebacate, DEHS). The result is shown in Figure 3.2.2.

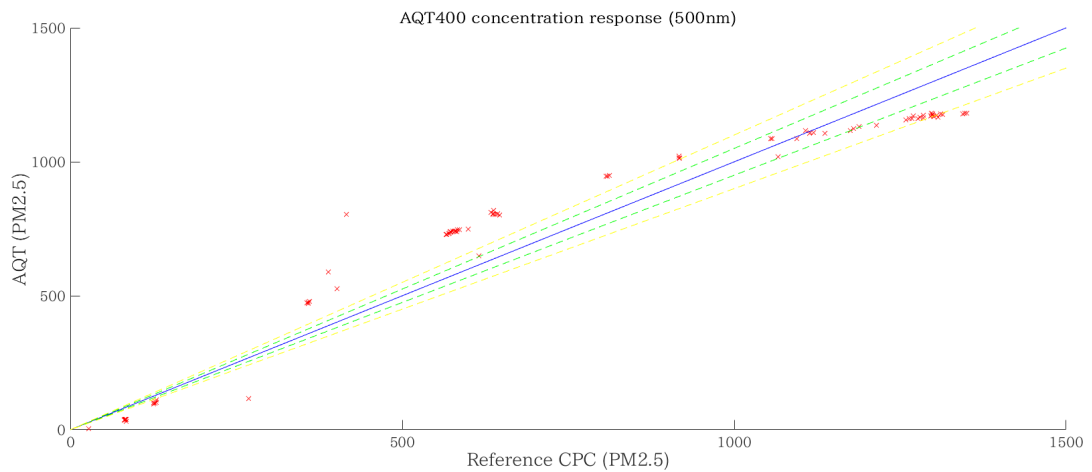


**Figure 3.2.2** The response of the AQT 420 to a variable mass concentration, when the particles are monomodal 500 nm organic particles.

In the second calibration, we directed variable sized aerosol particles to the AQT and to the reference CPC. The aim was to determine the cut-off diameter of the optical counter in the AQT. This is presented in Figure 3.2.3.

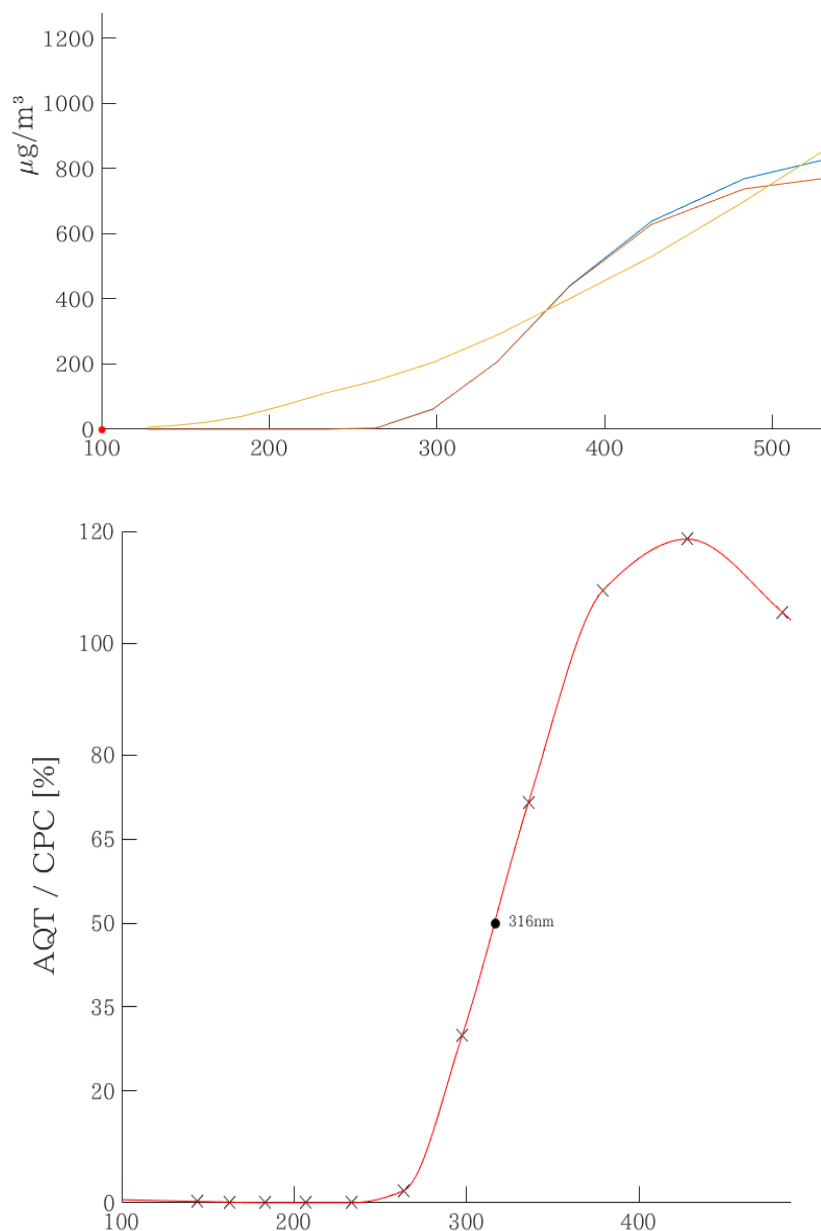


**Figure 3.2.3** Top panel shows the response of the AQT sensor to different sized particles against the SCAR derived mass concentration. The mass with the reference system is converted from number concentration assuming the density of the organic surfactant. Lower panel describes the ratio between the mass concentrations. The AQT 420 optics are able to detect 50% of the mass, when the particles are 320 nm in diameter. In this experiment the AQT 420 was not able to detect mass concentrations larger than  $1000 \mu\text{g}/\text{m}^3$  and therefore the cut-off curve deviates in the larger sizes.

As a summary, the AQT420 was able to detect aerosol particles down to 250 nm in size. In the subsequent laboratory tests, we used a prototype optics for the AQT 420 with blue laser (405 nm wavelength). In these tests the lowest detectable particles were 200 nm in diameter (Järvinen, 2018). The results showed that perpendicular polarized laser has a five-fold larger scattering cross section compared with parallel polarized laser (Järvinen et al. 2018). There is definitely potential in improving the optics of the AQT 420 sensor towards detecting smaller particles.

## 4. Atmospheric measurements

### 4.1 Side-by-side intercomparison against the reference method and performance against AQ-directive

The performance of the AQT-420 sensors (2017 Release) against the reference method for particulate matter was tested with the side-by-side comparison of AQT-420 sensors against the reference method. The reference method that was used followed the standard method for PM<sub>2.5</sub> and PM<sub>10</sub> (EN 12341, 2014). The comparison took place at Mäkelänkatu station in Helsinki for both PM<sub>2.5</sub> and PM<sub>10</sub> size fraction during March 20 to June 1, 2018. The campaign covered the period where high concentrations of PM<sub>10</sub> was expected due to the resuspension of the winter sand from the roads and walk sides.

At the station three identical AQT-420 sensors were installed on the roof of the measurement cabin. Two identical sampling system, Derenda Low Volume Sequential Samplers by Comde Derenda were used to collect the 24-hour samples, one equipped with PM<sub>2.5</sub> inlet and the other for PM<sub>10</sub> inlet. The samplers fulfil the criteria of the EN 12341 standard with the both type of inlet design as well as for the filter storage conditions during sampling. The handling, conditioning and weighing system of the filters is described in more details elsewhere (Waldén et al. 2017).

The automated PM-analyzer used for the measurement of continuous mass concentrations of PM<sub>2.5</sub> and PM<sub>10</sub> in ambient air at the station was TEOM 1405 by Thermo Scientific Instrument. It is based on the tapered element oscillating microbalance technique to measure the concentration of the particulate matter in the air. It is a direct mass measurement technique on a filter with real-time data output. The instrument is a single size class analyzer which can be equipped with size selective inlet either for measurement of PM<sub>2.5</sub> or PM<sub>10</sub> size fraction. The TEOM 1405 was equipped for PM<sub>10</sub> measurements by US-EPA design and for PM<sub>2.5</sub> measurements a combination of PM<sub>10</sub> inlet by US-EPA design and the sharp cut off cyclone. The instrument was tested for equivalent method with the reference method (Waldén et al, 2017) and took also part in the verification study (Waldén and Vestenius, 2018). The calibration factors to correct the results against the reference method was in use at the Mäkelänkatu site for both of the TEOM 1405 instruments.

The data analysis for the comparison study of AQT-420 sensors against the reference method for the PM<sub>2.5</sub> and PM<sub>10</sub> size fraction was made according to the guidance document "Guide to the Demonstration of Equivalence of Ambient Air Monitoring Methods", (GDE, 2010). The time series of hourly and daily averages for PM<sub>2.5</sub> and PM<sub>10</sub> comparison measurements are presented in Figures 4.1.1 and 4.1.2. To demonstrate the agreement between the PM-concentration obtained by sensor and the result obtained by the reference method is made with the orthogonal regression analysis (Beijk et al. 2006). Following the GDE-procedure the raw data can be corrected against the reference method and then to demonstrate, if the corrected results agree with the results of the reference method within the expanded uncertainty defined by the AQ-directive, (AQD 2008/50/EC, 2008) see in Figures 2.3.3 – 2.3.4 for the AQT-420 sensors 1-3 and the TEOM 1405 for the PM<sub>2.5</sub>. The similar figures are presented for PM<sub>10</sub> comparison in Figures 4.1.5 – 4.1.6.

The uncertainty between the results from the sensor and the results of the reference method was calculated from the variance of the slope and intercept of the orthogonal regression analysis. Expanded uncertainty was then calculated as  $2 \times \sigma_c$ , where  $\sigma_c$  is the combined uncertainty of the variances of the slope and intercept. The expanded uncertainty is expressed as relative value of the

absolute value divided by the relevant limit value, e.g. for PM10 it is  $50 \mu\text{g}/\text{m}^3$  as daily average value. The achieved value for the relative expanded uncertainty is then compared with the requirement of the AQ-directive which for the indicative measurement method, like in case of sensor, is less than 50 %. The results of the regression analysis are presented in Table 4.1.1 for PM2.5 and in Table 4.1.2 for PM10.

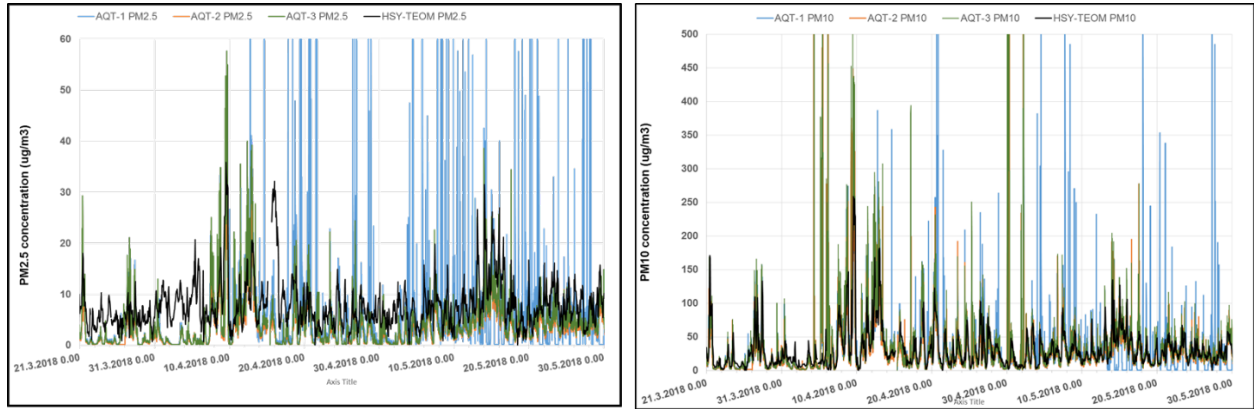


**Figure 4.1.1.** Time series of 1-hour averages of PM2.5 (on the left) and PM10 (on the right) for AQT-420 sensors 1 – 3 and continuous PM-analyzer, TEOM 1405.

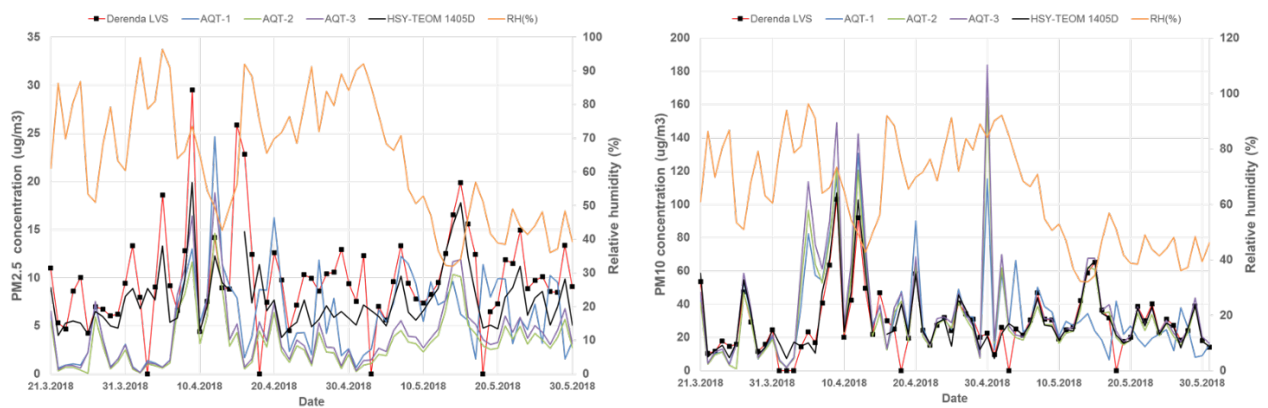


**Figure 4.1.2.** Time series of daily averages of PM2.5 (on the left) and PM10 (on the right) for AQT-420 sensors (AQT1 – 3), continuous site PM-analyzer, (HSY-TEOM 1405) and the reference method (Derenda LVS). The relative humidity is also presented, scale on the right.

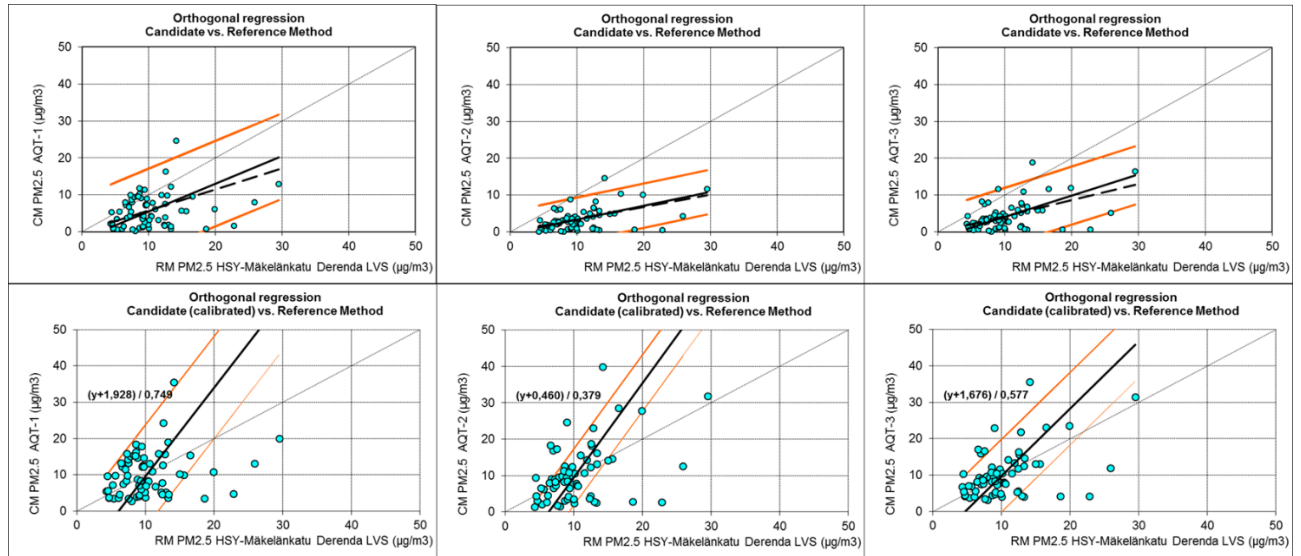


**Figure 4.1.3.** The scatter plot for the AQT-1-3 sensors against the reference method for PM2.5 measurements with the uncorrected results (figures on the top) and the corrected results including the correction equation (figures below) by the orthogonal regression analysis.

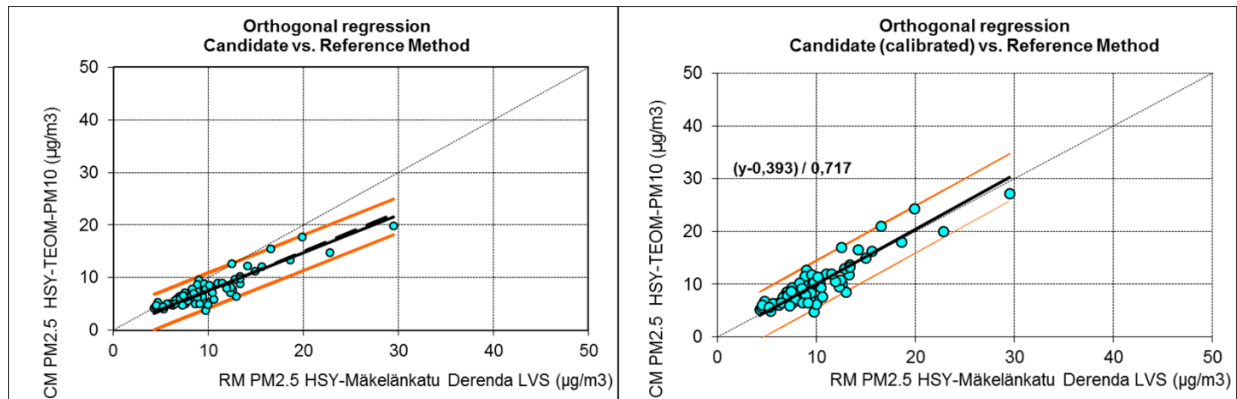


**Figure 4.1.4.** The scatter plot for the TEOM 1405 against the reference method for PM2.5 measurements with the uncorrected results (on the left) and the corrected results including the correction equation (on the right) by the orthogonal regression analysis.

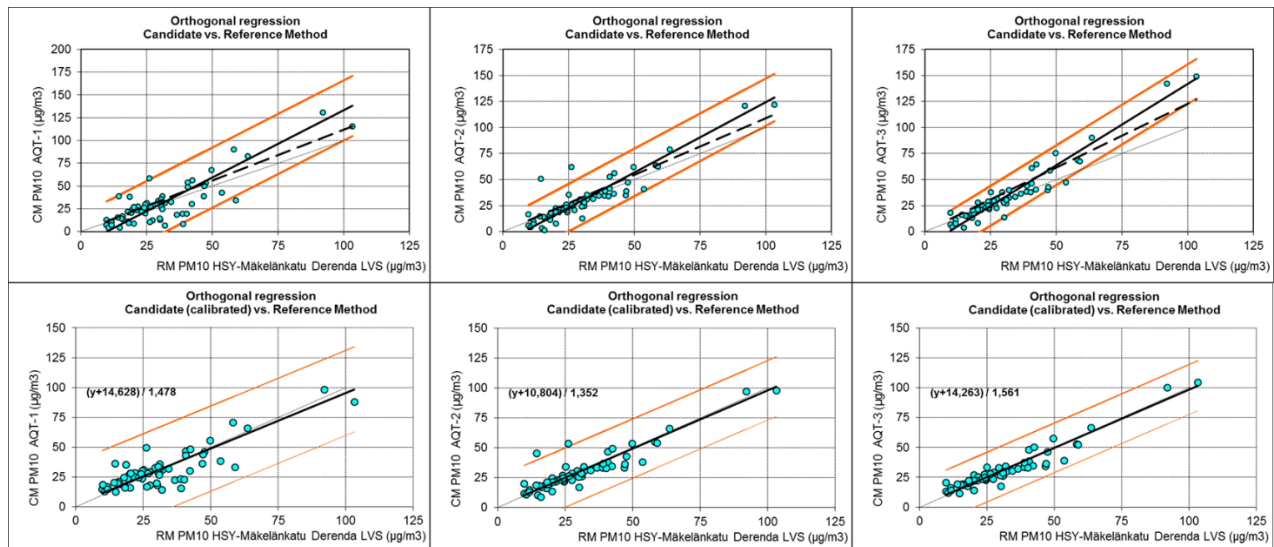


**Figure 4.1.5.** The scatter plot for the AQT-1-3 sensors against the reference method for PM10 measurements with the uncorrected results (figures on the top) and the corrected results including the correction equation (figures below) by the orthogonal regression analysis.

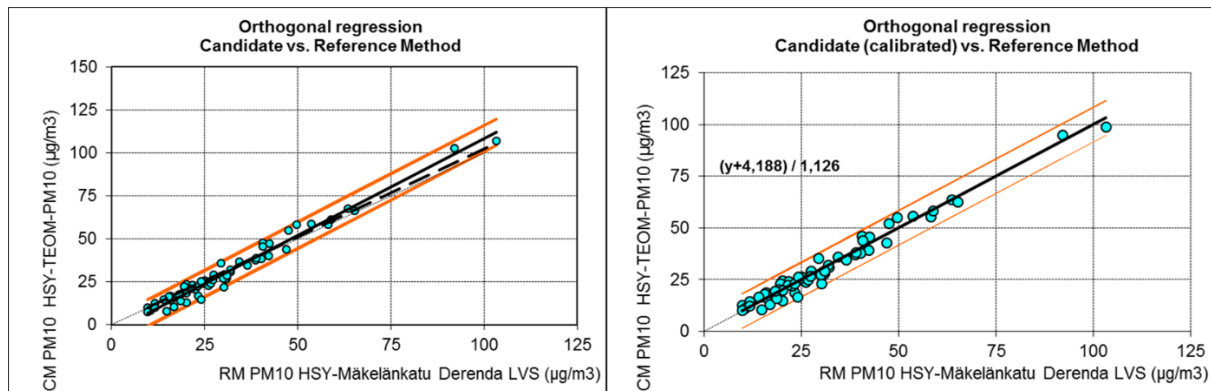


**Figure 4.1.6.** The scatter plot for the TEOM 1405 against the reference method for PM10 measurements with the uncorrected results (on the left) and the corrected results including the correction equation (on the right) by the orthogonal regression analysis.

**Table 4.1.1.** A summary of results from the regression analysis for PM2.5 comparisons of the AQT-420 sensors 1 – 3 and the TEOM 1405 against the reference method with the raw data and the calibrated data. The red font indicates where the requirements are not met.

	HSY-TEOM-PM2.5	AQT-420-1	AQT-420-2	AQT-420-3	AQT-420-1-3 <sub>Ave</sub>
<b>REGRESSION RESULTS (RAW)</b>					
Slope b	0,7165	0,7486	0,3790	0,5769	0,4603
Slope b forced through origin	0,3929	-1,9280	-0,4598	-1,6765	0,4391
Number of data points	68	70	70	70	70
Expanded relative uncertainty	54,8%	71,4%	128,4%	98,4%	111,6%
<b>EQUIVALENCE TEST (CALIBRATED)</b>					
Calibration equation (line)	1,396y - 0,548	1,336y + 2,575	2,639y + 1,213	1,733y + 2,906	2,173y + 0,534
Calibration equation (slope)	1,334y	1,748y	2,94y	2,31y	2,278y
Number of data points	68	70	70	70	70
Expanded relative uncertainty, U	16,5%	206,8%	221,7%	125,0%	250,4%

**Table 4.1.2.** A summary of results from the regression analysis for PM10 comparisons of the AQT-420 sensors 1 – 3 and the TEOM 1405 against the reference method with the raw data and the calibrated data. The red font indicates where the requirements are not met.

	HSY-TEOM-PM10	AQT-420-1	AQT-420-2	AQT-420-3	AQT-420-1-3 <sub>Ave</sub>
<b>REGRESSION RESULTS (RAW)</b>					
Slope b	1,1260	1,4783	1,3523	1,5611	1,4031
Intercept	-4,1881	-14,6283	-10,8038	-14,2627	-12,1320
Number of data points	66	63	63	61	61
Expanded relative uncertainty	15,6%	68,5%	48,1%	64,4%	45,6%
<b>EQUIVALENCE TEST (CALIBRATED)</b>					
Calibration equation (line)	0,888y + 3,719	0,676y + 9,895	0,739y + 7,989	0,641y + 9,136	0,713y + 8,647
Calibration equation (slope)	0,976y	0,894y	0,917y	0,814y	0,895y
Number of data points	66	63	63	61	61
Expanded relative uncertainty, U	12,9%	44,4%	33,5%	25,5%	26,8%

## 4.2 Correction factors for the AQT 420 sensors (2017 Release)

All the Vaisala AQT-420 sensors were brought to Mäkelänkatu supersite for roughly month-long side-by-side comparison test during the Autumn and Winter 2017. The reference reference instrument for PM10 and PM2.5 was TEOM 1405, and for NO<sub>2</sub>, O<sub>3</sub> and CO Horiba Apna 370, Horiba ApoA-370 and Horiba APMA-360, respectively. The reference instruments at Mäkelänkatu are operated by HSY. In the following, the sensors are named by the location where they are installed outside the comparison period. The testing periods for the different sensors are shown in Table 4.2.1. When the sensors were brought to Mäkelänkatu, it took some time before the sensors started recording the concentrations of gaseous components in a reasonable manner. Thus, for gaseous components, some data from the beginning of the measurement periods were removed for each instrument. Additionally, some outliers were removed.

**Table 4.2.1** Side-by-side test periods for the Vaisala AQT-420 sensors (2017 Release) at Mäkelänkatu site. The sensors are named according to the location where they are outside the test period.

Measurement Period	Sensor
2017-07-17 – 2017-08-28	Hiekkaharju
2017-09-22 – 2017-10-20	Laaksolahti, Olari, Pakila, Rekola
2017-10-20 – 2017-11-16	Kaivoksela VT3, Mannerheimintie, Pirkkola VT3, Sörnäinen, Suutarila – Kehä III, Vallikallio – Kehä I
2017-11-17 – 2017-12-18	Itä-Hakkila, Jätkäsaari, Latokaski, Malmi, Myyrmäki, Pakila (vara)

The correction factors for the sensors were determined as linear least squares fits, with slope  $S$  and intercept  $I$ , to the concentration observed with the sensor ( $C_{\text{sensor}}$ ) against the concentration from the reference instrument ( $C_{\text{reference}}$ ), as in

$$C_{\text{sensor}} = S \times C_{\text{reference}} + I. \quad (\text{Eq. 1})$$

The correction factors for the sensors were calculated from these values as

$$CF_1 = 1/S$$

and

$$CF_2 = -I/S,$$

and they should be applied to correct the concentration detected with the sensor as

$$C_{\text{corrected}} = CF_1 \times C_{\text{sensor}} + CF_2. \quad (\text{Eq. 2})$$

In the next section we explore the correlation between the AQT 420 Sensor (2017 Release) and ambient data from the reference instruments.

#### 4.2.1 NO<sub>2</sub> concentrations

The sensors showed good response to the NO<sub>2</sub> concentrations in general. Figure 4.2.1 shows the sensors with the highest (on the left) and the lowest (on the right) correlation with respect to the reference instrument during each testing period. The lowest correlation, with  $R^2 = 0.72$ , was observed for the Laaksoalahti sensor. The difference between Laaksoalahti and other sensors was quite significant, taken that all other sensors showed correlation coefficients  $R^2$  in range 0.83-0.90.

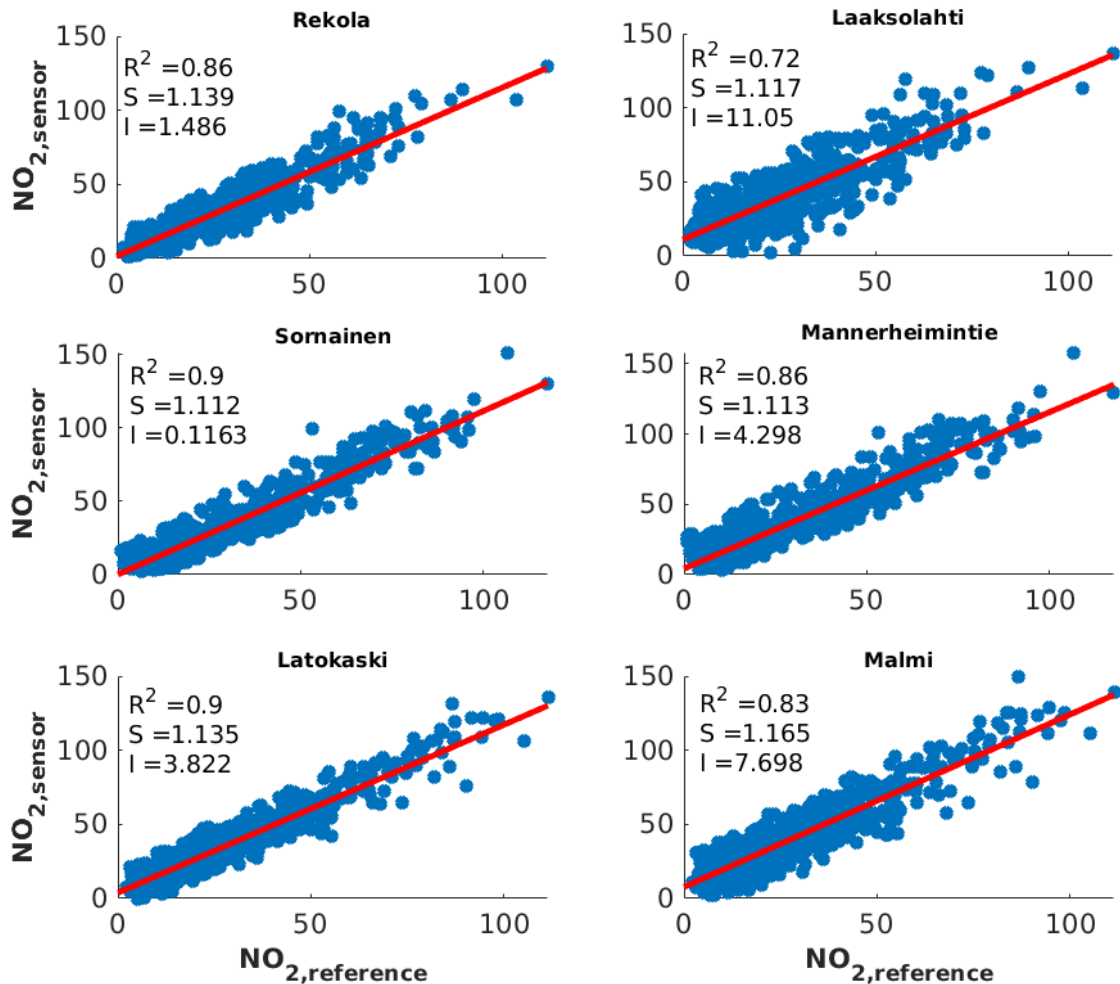


**Figure 4.2.1.** NO<sub>2</sub> concentrations measured with the sensors vs the reference measurement at the Mäkelänkatu site. The panel title indicates the sensor in question. Each row represents a testing period, the highest row showing the August and September periods, middle row the October period and the lowest row the November period. Left hand side sensors showed the highest and on the right hand side sensors the lowest correlation coefficients ( $R^2$ ) during the test period. The other instruments had  $R^2$  values within this range.

The sensors showed very similar slope values determined with the linear least squares fitting. The slopes varied between 1.10 and 1.17 for all sensors except Kaivoksela VT3 (slope 1.23) and Pakila (slope 1.07) (see Table Y). It is notable that these two sensors did not variate from the other sensors in terms of the correlation coefficient (Figure 2.3.8).

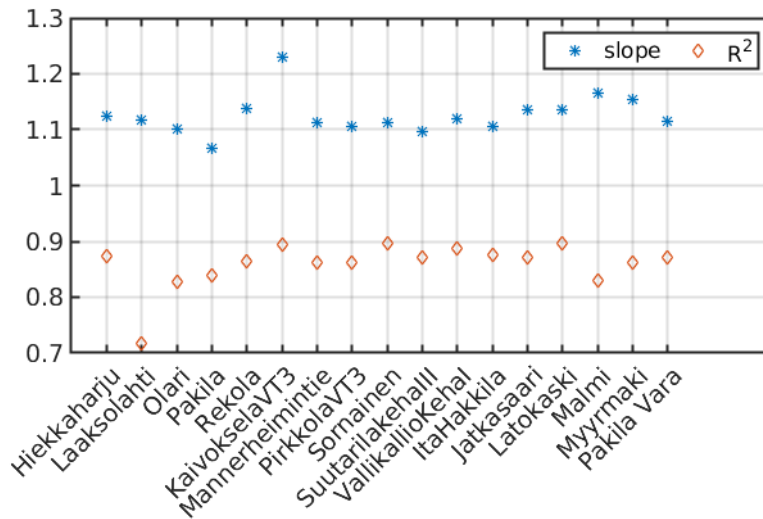


**Figure 4.2.2.** Slope values for NO<sub>2</sub> in sensor vs. reference linear least squares fits and the related correlation coefficients R<sup>2</sup>.

The correction factors for NO<sub>2</sub> concentrations detected with the AQT420 sensors, determined as in Eq. 2, are presented in Table 4.2.2. The variation of the slope-factors CF1 is small and all the intercept-factors CF2 are negative.

**Table 4.2.2.** The determined correction factors for NO<sub>2</sub> concentrations detected with the AQT420 sensors.

Sensor	CF <sub>1</sub>	CF <sub>2</sub>	R <sup>2</sup>
Hiekkaharju	0.890	-1.76	0.875
Laaksolehti	0.895	-9.89	0.717
Olari	0.908	-2.56	0.828
Pakila	0.937	-1.25	0.839
Rekola	0.878	-1.31	0.863
Kaivoksela VT3	0.813	-1.36	0.894
Mannerheimintie	0.898	-3.86	0.863
Pirkkola VT3	0.904	-4.36	0.863
Sörnäinen	0.899	-0.10	0.897
Suutarila - Kehä III	0.912	-4.09	0.871
Vallikallio – Kehä I	0.894	-2.74	0.888
Itä-Hakkila	0.905	-4.14	0.876
Jätkäsaari	0.880	-3.43	0.871
Latokaski	0.881	-3.37	0.896
Malmi	0.858	-6.61	0.830
Myyrmäki	0.867	-5.97	0.862
Pakila (vara)	0.896	-3.03	0.871

#### 4.2.2 CO concentrations

The sensors showed relatively good response to the CO concentrations (Figure 4.2.3), but the correlations were typically slightly lower than for NO<sub>2</sub>. The correlation coefficients R<sup>2</sup> varied between 0.71 and 0.88, the worst correlation being observed with the “Pakila vara” sensor and the best with the Laaskolahti sensor. It is notable that the Laaskolahti sensor showed clearly the weakest correlation for NO<sub>2</sub>. The high correlation in CO concentrations suggests that the reason for low correlation for NO<sub>2</sub> is not due to installation or other problem, but is directly related to the NO<sub>2</sub> sensor.

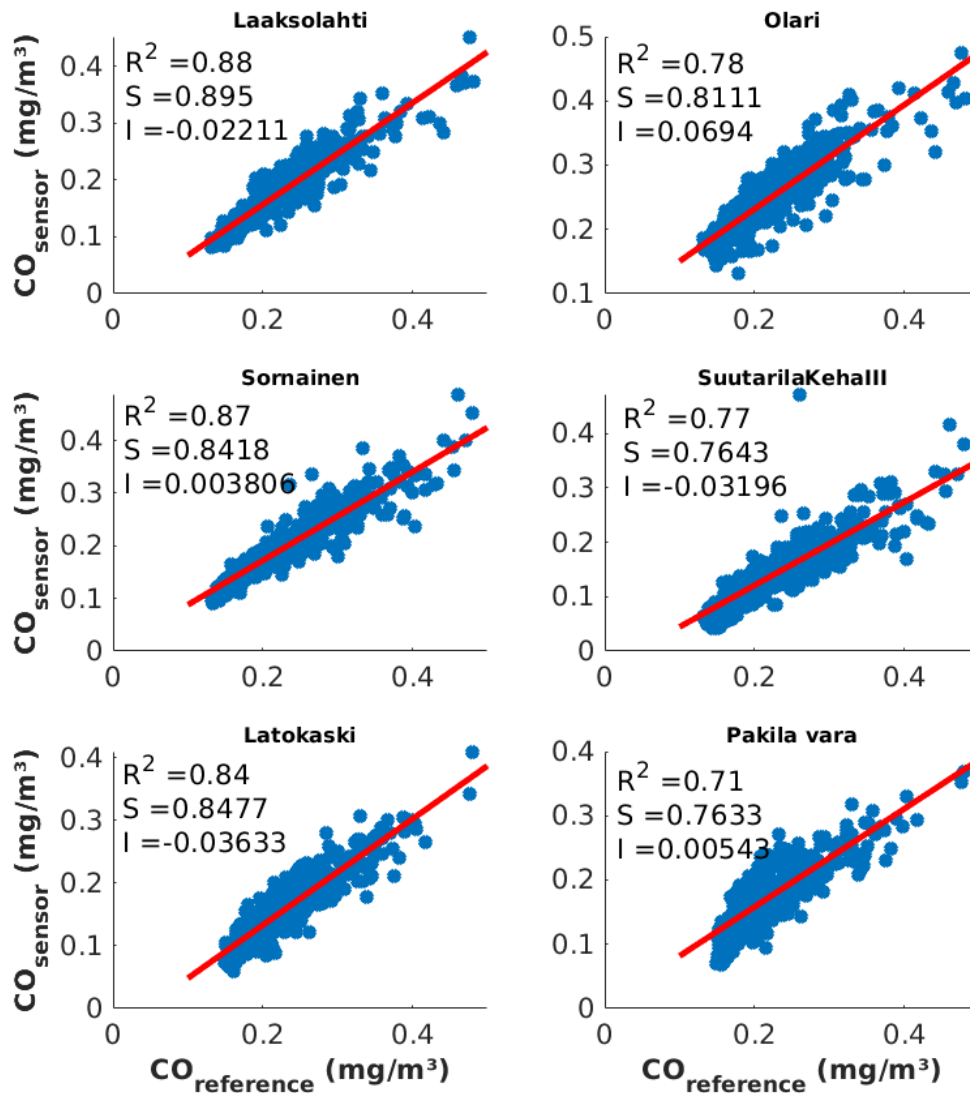


**Figure 4.2.3.** CO concentrations measured with the sensors vs the reference measurement at the Mäkelänkatu site. The panel title indicates the sensor in question. Each row represents a testing period, the highest row showing the August and September periods, middle row the October period and the lowest row the November period. Left hand side sensors showed the highest and the right hand side sensors the lowest correlation coefficients (R<sup>2</sup>) during the test period. The other instruments had R<sup>2</sup> values within this range.

The slopes in the sensors vs reference concentrations during the comparison period are depicted in Fig. 2.3.10. and the calculated correction factors are presented in Table 2.3.5. Interestingly, the slopes seem to have a decreasing trend from the August period (Hiekkaharju) and September period (Laaksolahti to Rekola) towards October (Kaivoksela to Vallikallio) and November (Itä-Hakkila to Pakila vara). In order to investigate this further, we investigated the ratio of the sensor and reference concentration as a function of temperature.

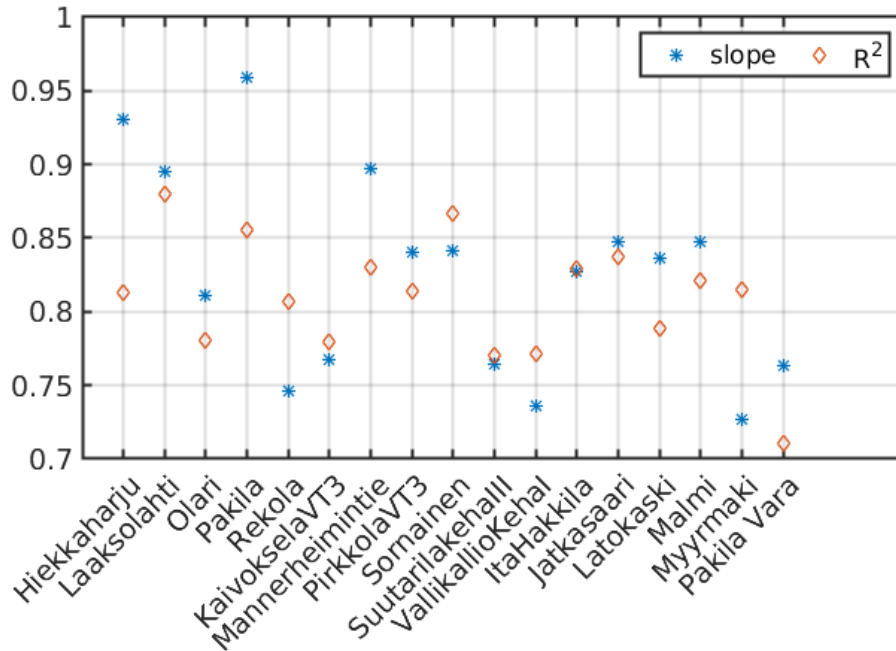


**Figure 4.2.4.** Slope values for CO in sensor vs. reference linear least squares fits and the related correlation coefficients R<sup>2</sup>.

**Table 4.2.3.** The determined correction factors for CO concentrations detected with the AQT420 sensors.

Sensor	CF <sub>1</sub>	CF <sub>2</sub> [mg/m <sup>3</sup> ]	R <sup>2</sup>
Hiekkaharju	1.07	0.0158	0.813
Laaksolahti	1.12	0.0247	0.880
Olari	1.23	-0.0856	0.781
Pakila	1.04	0.0343	0.855
Rekola	1.34	-0.0226	0.807
Kaivoksela VT3	1.30	-0.0216	0.779
Mannerheimintie	1.11	0.0456	0.830
Pirkkola VT3	1.19	0.0493	0.814
Sörnäinen	1.19	-0.0045	0.867
Suutarila - Kehä III	1.31	0.0418	0.770
Vallikallio – Kehä I	1.36	0.0150	0.772
Itä-Hakkila	1.21	0.0330	0.829
Jätkäsaari	1.18	0.0429	0.837
Latokaski	1.20	0.0218	0.788
Malmi	1.18	0.0290	0.821
Myyrmäki	1.38	-0.0697	0.815
Pakila (vara)	1.31	-0.0071	0.711

We observed that in most of the sensors the CO concentration is sensitive to temperature. In Figure 4.2.5. we present the ratios of the CO concentration from the reference instrument and the corrected sensor concentration (corrected with Eq. 2 and CF values from Table 4.2.3) for each sensor. Most of the sensors show a negative correlation between this ratio and temperature when the temperature is above 5 °C and positive correlation when the temperature is below this (Table 4.2.6). Finally, we determined general temperature correction factors for these temperature ranges as averages of the

slope and intercept values in Table 4.2.4 The temperature adjusted correction functions for CO sensors resulted as

$$[CO]_{corrected,T} = (CF_1 \times [CO]_{sensor} + CF_2) \times (-0.0285 \times T(^{\circ}C) + 1.27) \quad \text{for } T > 5^{\circ}C$$

and

$$[CO]_{corrected,T} = (CF_1 \times [CO]_{sensor} + CF_2) \times (0.0299 \times T(^{\circ}C) + 0.947) \quad \text{for } T < 5^{\circ}C,$$

where CF1 and CF2 are the sensor specific correction factors from Table 4.2.3. By applying this temperature correction, the correlations between reference and corrected CO concentration improved for all sensors except Pirkkola and Sörnäinen (Table 2.3.4. and Figure 4.2.6.).

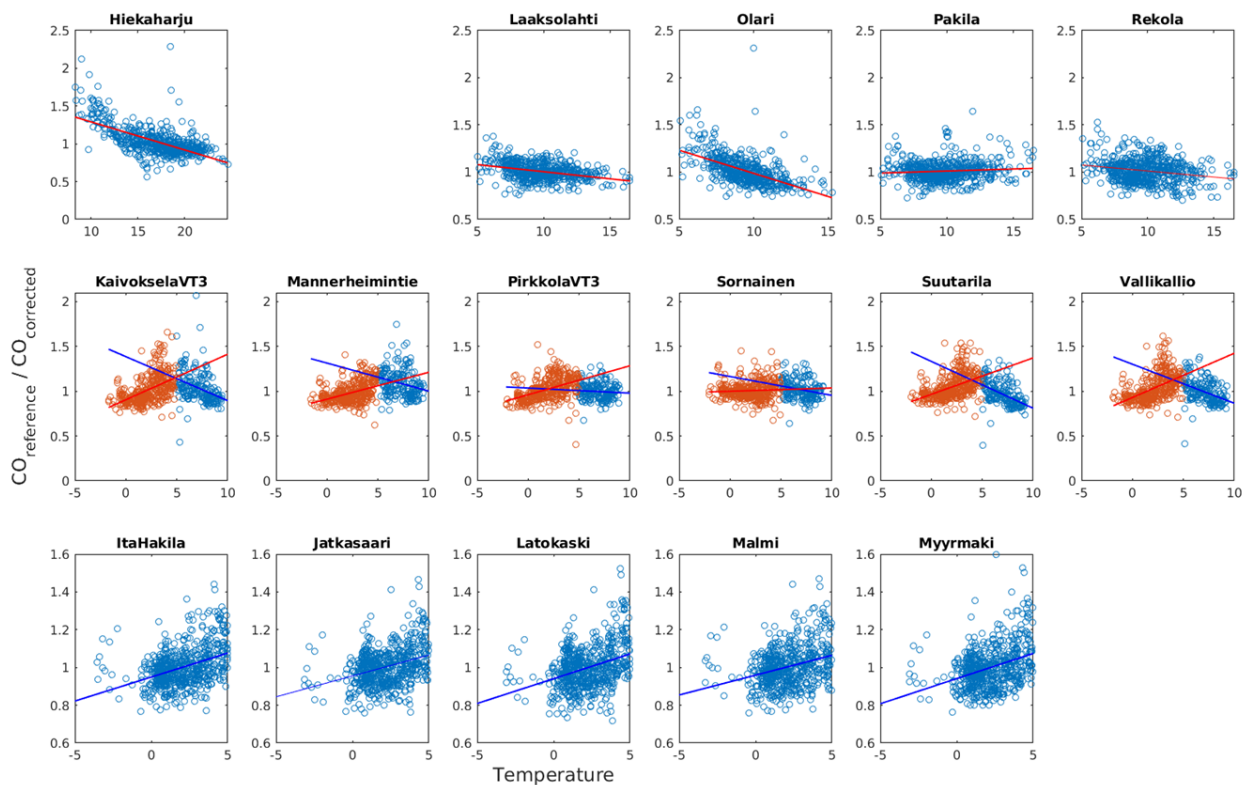


**Figure 4.2.5.** Relative biases between the CO concentration from sensors and the reference instruments presented as functions of temperature. The sensor concentrations are corrected with the linear correction factors given in Table 2.3.5.

**Table 4.2.4.** Linear least squares fit parameters to and correlation coefficients for the CO concentration relative biases (depicted in Fig. 2.3.11, fits represented with lines) as functions of temperature.

	T > 5 °C			T < 5 °C		
	S <sub>T1</sub>	I <sub>T1</sub>	R <sup>2</sup>	S <sub>T2</sub>	I <sub>T2</sub>	R <sup>2</sup>
Hiekkaharju	-0.0372	1.6635	0.395			
Laaksolehti	-0.0151	1.1556	0.125			
Olari	-0.0491	1.4783	0.310			
Pakila	0.0043	0.9687	0.008			
Rekola	-0.0128	1.1408	0.046			
Kaivoksela VT3	-0.0491	1.3864	0.126	0.0508	0.9054	0.247
Mannerheimintie	-0.0313	1.3145	0.068	0.0300	0.9118	0.163
Pirkkola VT3	-0.0057	1.0359	0.005	0.0323	0.9616	0.192
Sörnäinen	-0.0211	1.1643	0.055	0.0036	1.0000	0.004
Suutarila - Kehä III	-0.0523	1.3336	0.227	0.0407	0.9656	0.214
Vallikallio – Kehä I	-0.0436	1.3020	0.165	0.0494	0.9303	0.252
Itä-Hakkila				0.0254	0.9494	0.158
Jätkäsaari				0.0221	0.9551	0.117
Latokaski				0.0262	0.9406	0.122
Malmi				0.0210	0.9594	0.093
Myyrmäki				0.0266	0.9411	0.131

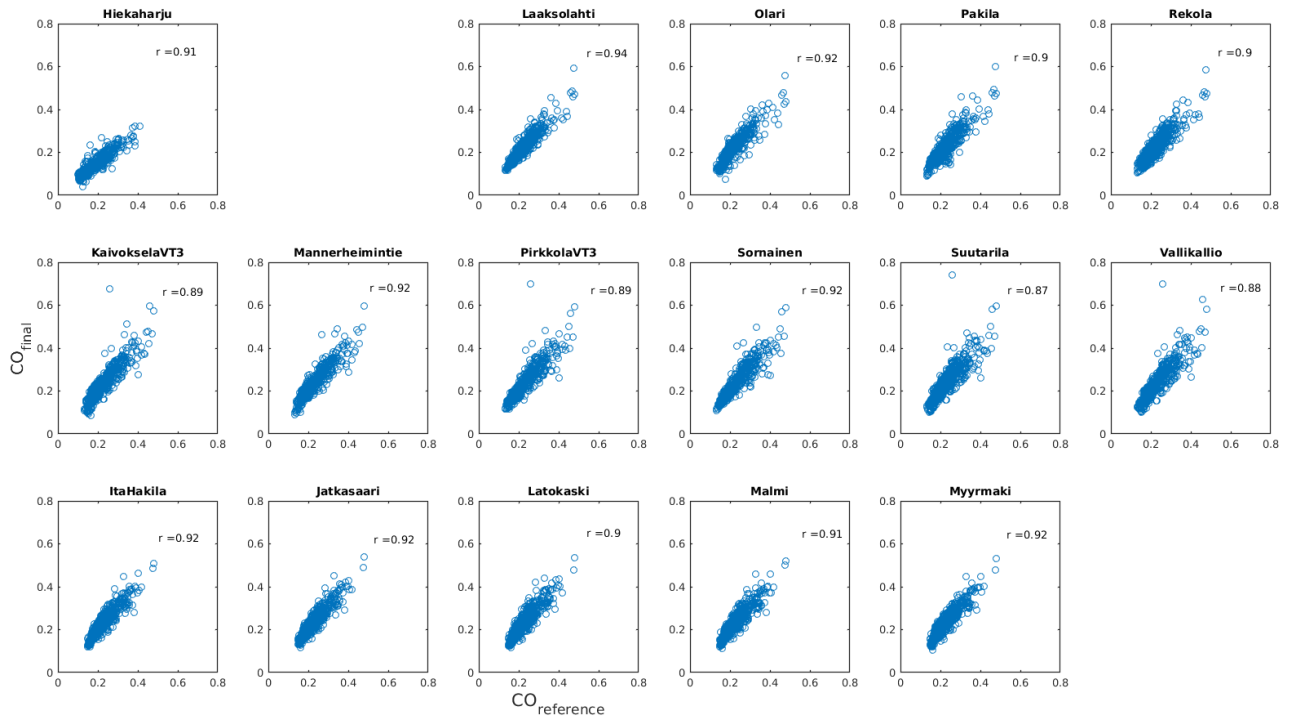


**Figure 4.2.6.** CO concentrations from the sensors adjusted with the average linear correction factors (Table 2.3.5) and average temperature dependent correction factors (determined from Table 2.3.6, average values presented in text.

### 4.2.3 Ozone

The correlations between different sensors and the reference instrument varied more than in case of other pollutants, from  $R^2$  below 0.3 to over 0.7 (Figures 4.2.7 and 4.2.8. and Table 4.2.5). The correlation seemed to correlate with the slope value especially during the November test period (Fig. 2.3.17), and this seems to be related to relatively good correlation during parts of the test periods, but varying intercepts between these parts. This is visible as distinct stripes with apparently close to similar slope but different intercepts, especially in the panels for Sörnäinen, Suutarila and Latokaski sensors in Figure 4.2.8. We investigated if this could be related to temperature (Figure 4.2.8), but the results were mixed: some sites showed correlation while some did not, and the sensors tended to underestimate the concentrations under higher temperature in September test period and overestimate under higher temperature in October test period. Further investigation on this topic could reveal some reasons for the observed behavior.

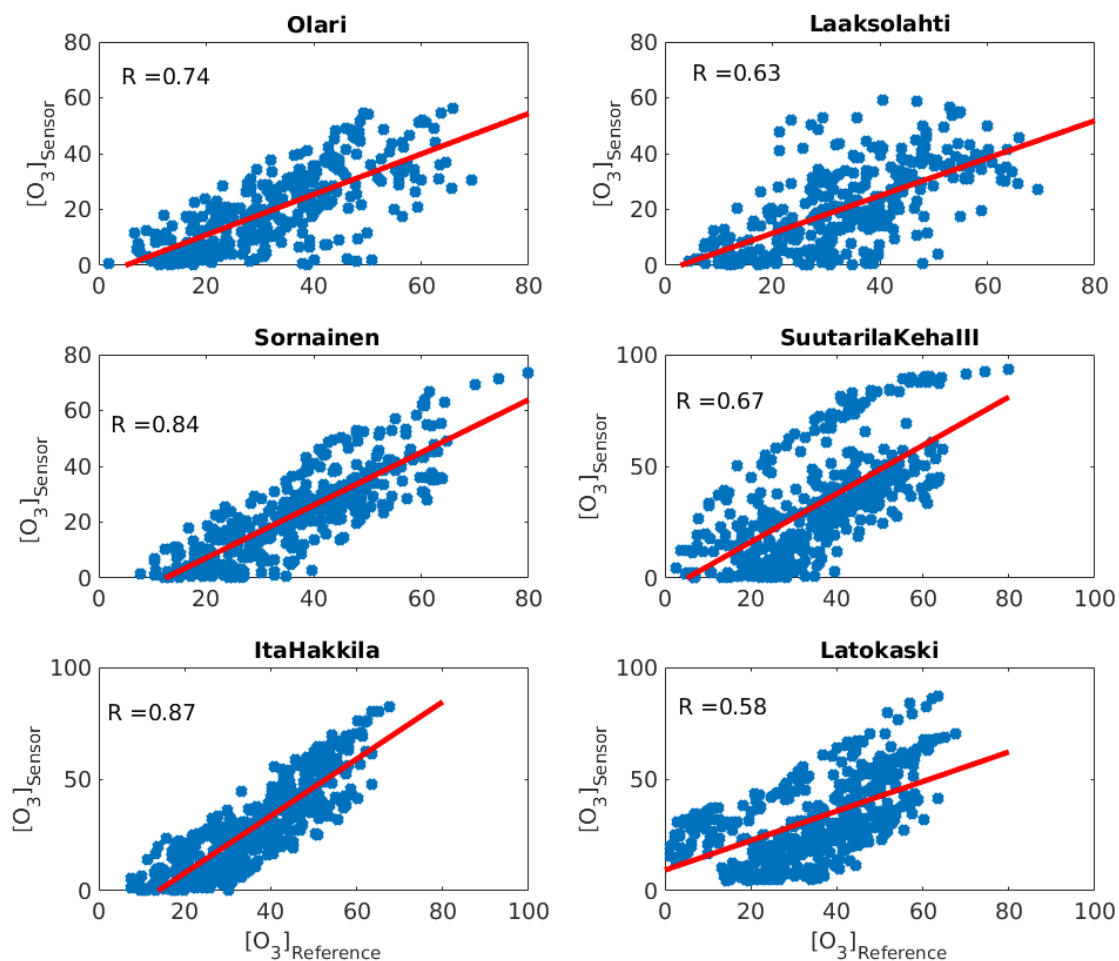


**Figure 4.2.7.** O<sub>3</sub> concentrations measured with the sensors vs the reference measurement at the Mäkelänkatu site. The panel title indicates the sensor in question. Each row represents a testing period, the highest row showing the August and September periods, middle row the October period and the lowest row the November period. Left hand side sensors showed the highest and the right hand side sensors the lowest correlation coefficients during the test period. The other instruments had correlation coefficient values within this range.

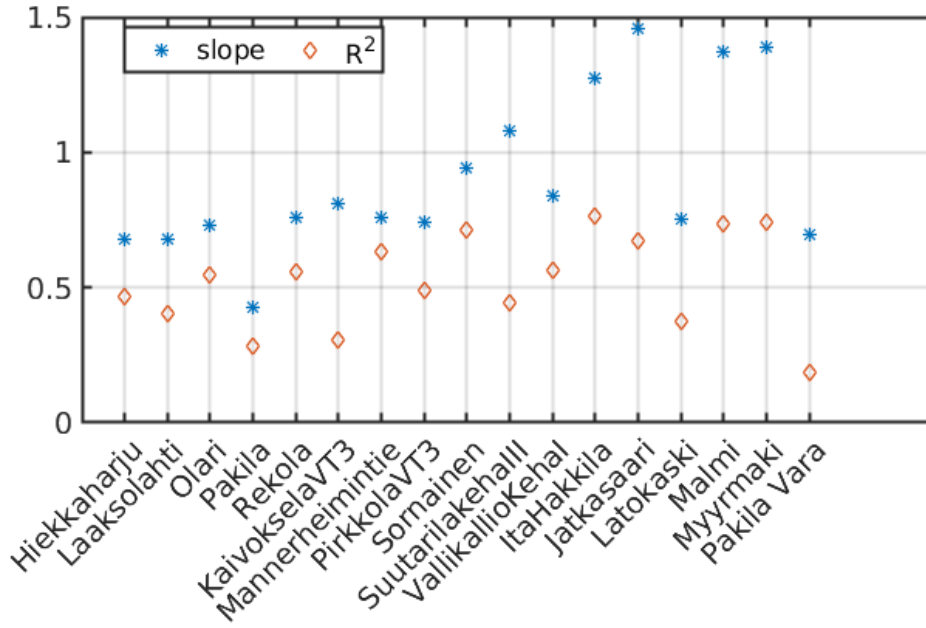


**Figure 4.2.8.** Slope values for O<sub>3</sub> concentrations in sensor vs. reference linear least squares fits and the related correlation coefficients R<sup>2</sup>.

**Table 4.2.5.** The determined correction factors for O<sub>3</sub> concentrations detected with the AQT420 sensors.

Sensor	CF <sub>1</sub>	CF <sub>2</sub>	R <sup>2</sup>
Hiekkaharju	1.47	14.8	0.469
Laaksolehti	1.47	3.32	0.405
Olari	1.38	5.22	0.547
Pakila	2.35	11.5	0.285
Rekola	1.32	4.94	0.559
Kaivoksela VT3	1.24	1.64	0.305
Mannerheimintie	1.32	13.0	0.633
Pirkkola VT3	1.35	8.55	0.487
Sörnäinen	1.06	12.4	0.712
Suutarila - Kehä III	0.925	5.08	0.446
Vallikallio – Kehä I	1.19	14.8	0.563
Itä-Hakkila	0.785	13.7	0.762
Jätkäsaari	0.687	13.9	0.674
Latokaski	1.32	-5.43	0.372
Malmi	0.728	10.4	0.737
Myyrmäki	0.719	10.6	0.743
Pakila (vara)	1.43	-6.96	0.184

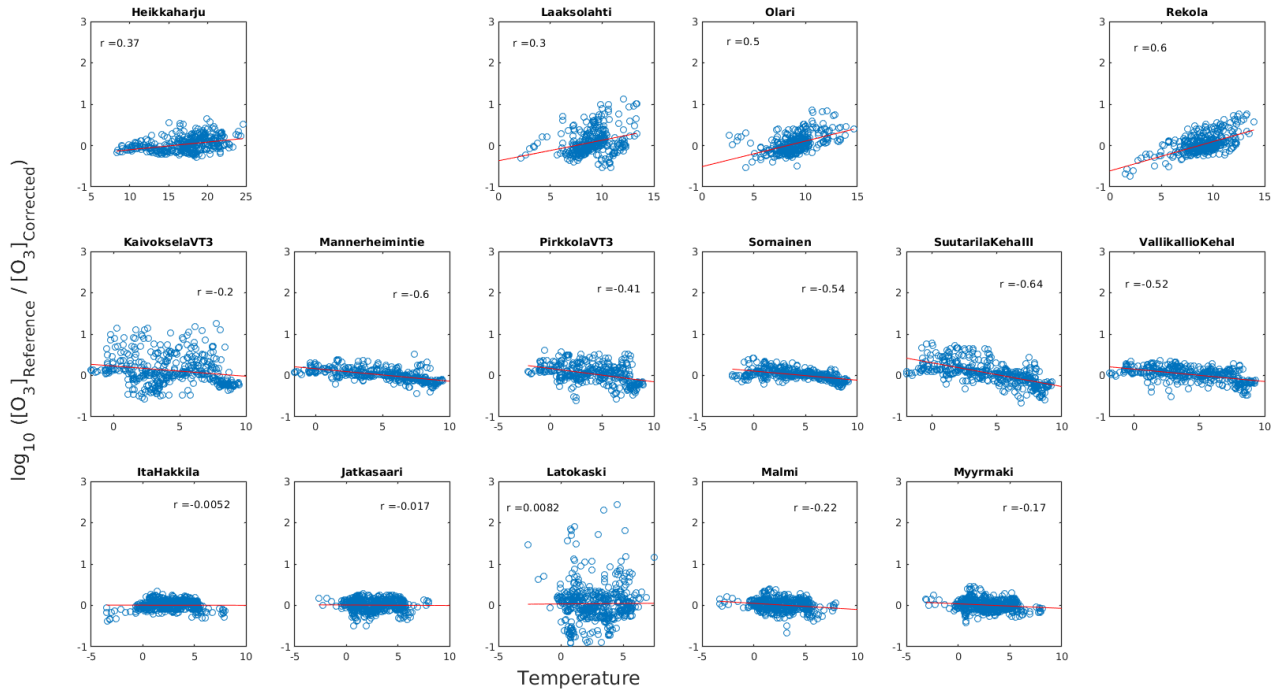


**Figure 4.2.8.** Relative biases between the O<sub>3</sub> concentration from sensors and the reference instruments presented as functions of temperature. The sensor concentrations are corrected with the linear correction factors given in Table 2.3.8.

#### 4.2.4 PM10

We compared the PM10 concentrations detected with the AQT420 sensors and the reference instruments both in linear and logarithmic scales (an example for Malmi sensor in Figure 4.2.9). Determining and applying correction factors with logarithmic scale is reasonable, if *i*) the concentration varies significantly (e.g. over an order of magnitude) and the low concentrations prevail for most of the time and *ii*) the purpose is to receive roughly accurate also for these low concentrations. While the PM10 concentration shows the variability as described in *i*) above, adjusting the correction factors with the linear scale is relevant, if it is the peak concentrations that are of the most interest.

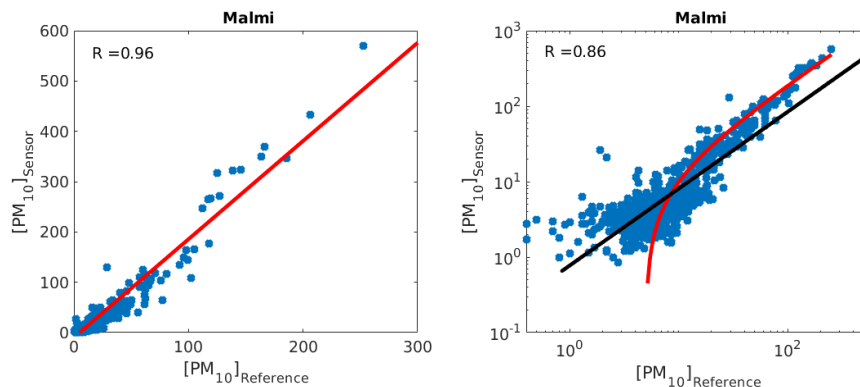


**Figure 4.2.9.** An example of the fitting of correction factors for AQT420 PM<sub>10</sub> from linear (left) and logarithmic (right) concentrations. The red line described the fit to the concentrations in linear scale and the black in logarithmic scale.

Figure 4.2.10 shows how the peak concentrations are captured much more accurately with the linear fit (top panel), but the low concentrations with the logarithmic fit (middle panel). The lowest panel shows in logarithmic scale the different nature of these fittings.

It would be possible to determine correction factors with a combined method, where the values below a certain threshold would be determined with a logarithmic fit and above the threshold with a linear fit. However, the continuity of the correction factors at the threshold should be carefully inspected. These kind of combined log-linear correction factors were not determined during this project, but could be investigated in future work.

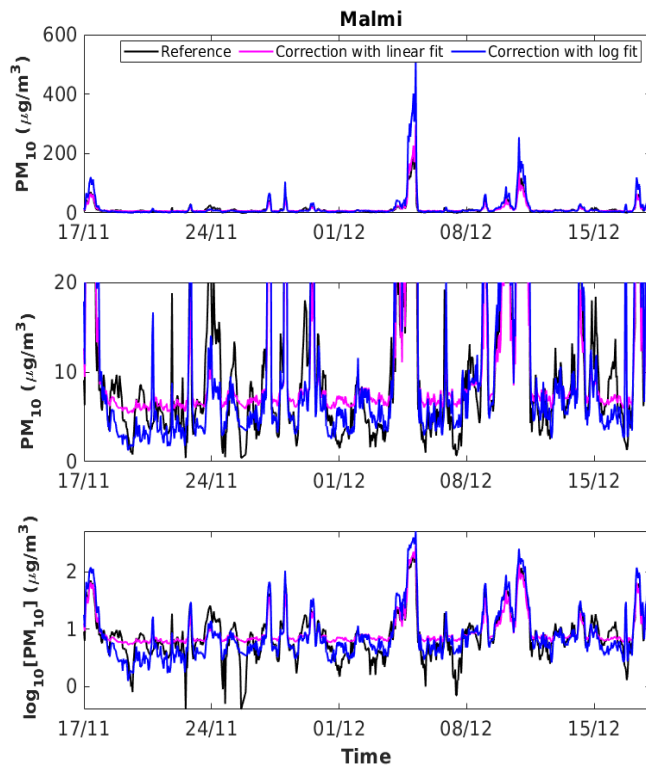


**Figure 4.2.10.** Comparison of linear and logarithmic correction factors to Malmi sensor with respect to the reference instrument. Top panel shows that the peak values are better captured with linear fit, and the middle panel (note the y-axis values) and the lowest panel (note the logarithmic y-axis values) show that the low values are much better captured with logarithmic fit.

Next, we present the PM10 correction factors in a similar manner than for the gases above, but both in logarithmic and linear scales. The sensors showing lowest and highest correlations during different comparison periods are depicted in figures N and M, and the slopes and correlation coefficients in Figure 4.2.11. The correction coefficients based on linear and logarithmic fittings are shown in Table 4.2.6. The correlations, both in linear and logarithmic scale, are clearly higher during the October and November comparison periods. The plausible reason for this is the higher PM10 concentrations during these months, which reduces the impact of instrument noise.

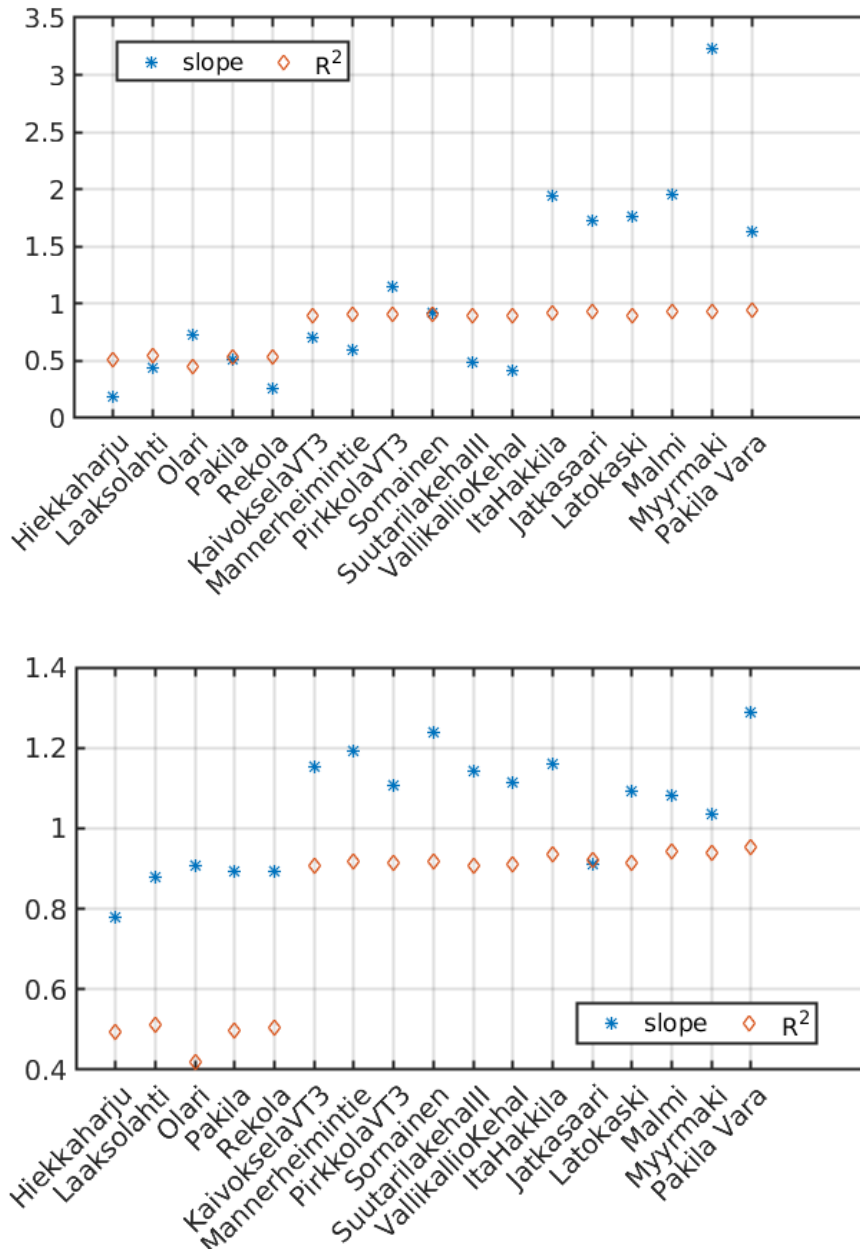


**Figure 4.2.11.** Slope values for linear (upper panel) and logarithmic (lower panel)  $PM_{10}$  concentrations in sensor vs. reference linear least squares fits and the related correlation coefficients  $R^2$ .

**Table 4.2.6.** The correction factors for PM<sub>10</sub> concentrations detected with the AQT420 sensors determined from logarithmic (on left) and linear (on right) concentrations.

Sensor	CF <sub>1</sub>	CF <sub>2</sub>	R <sup>2</sup>
Hiekkaharju	1.28	-0.482	0.495
Laaksolahti	1.14	-0.681	0.514
Olari	1.10	-1.01	0.420
Pakila	1.12	-0.766	0.496
Rekola	1.12	-0.379	0.505
Kaivoksela VT3	0.867	-0.275	0.908
Mannerheimintie	0.839	-0.188	0.919
Pirkkola VT3	0.904	-0.593	0.913
Sörnäinen	0.808	-0.219	0.918
Suutarila - Kehä III	0.875	-0.178	0.907
Vallikallio – Kehä I	0.899	-0.187	0.911
Itä-Hakkila	0.862	-0.396	0.936
Jätkäsaari	1.10	-1.35	0.923
Latokaski	0.915	-0.516	0.914
Malmi	0.925	-0.616	0.941
Myyrmäki	0.965	-1.28	0.940
Pakila (vara)	0.776	-0.203	0.953
Sensor	CF <sub>1</sub>	CF <sub>2</sub>	R <sup>2</sup>
Hiekkaharju	5.50	-3.24	0.516
Laaksolahti	2.25	-1.05	0.547
Olari	1.37	-1.44	0.455
Pakila	1.94	-1.32	0.531

Rekola	3.82	-1.08	0.536
Kaivoksela VT3	1.41	2.36	0.898
Mannerheimintie	1.67	2.90	0.911
Pirkkola VT3	0.87	1.34	0.907
Sörnäinen	1.08	3.80	0.904
Suutarila - Kehä III	2.06	3.57	0.894
Vallikallio – Kehä I	2.39	2.84	0.901
Itä-Hakkila	0.513	5.28	0.919
Jätkäsaari	0.581	3.81	0.938
Latokaski	0.568	4.89	0.901
Malmi	0.512	4.96	0.931
Myyrmäki	0.309	4.63	0.935
Pakila (vara)	0.614	5.26	0.942

#### 4.2.4.1 PM<sub>10</sub> and RH

We performed similar but extended analysis to PM<sub>10</sub> concentrations as a function of RH and temperature as presented above for CO and temperature. We observed that the sensors tended to underestimate the PM<sub>10</sub> concentrations more with increasing RH, but when RH approached 100 % the underestimation turned to overestimation especially during the November test period (Figure 4.2.12). We inspected this behavior further with dividing the data to different temperature bins, but the high non-linearities in the response of the sensor bias to RH made the parameterization of the bias in terms of T and RH complicated. Thus, we did not derive final parameterization for the sensor bias as a function of RH. In order to do this properly, one should inspect the raw data of the PM<sub>10</sub> sensor. The differences in different PM<sub>10</sub> size ranges should be inspected to determine their sensitivity to RH.

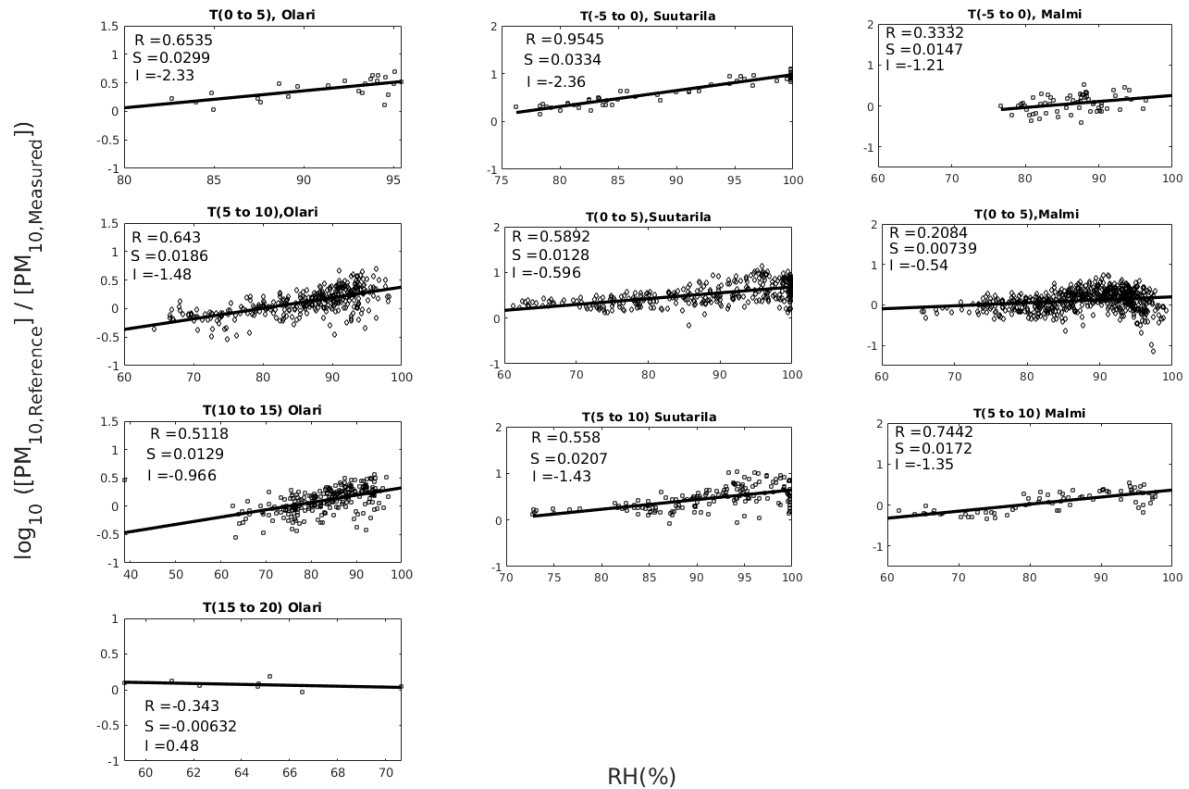


**Fig 4.2.12.** Logarithms of the ratio between PM10 concentrations from reference and example sensors as functions of relative humidity in different temperature bins (y-axis value 0 refers to same concentration, 1 to ten-fold underestimation by the sensor, 0.1 to ten-fold overestimation by the sensor). Olari sensor (left column) was at Mäkelänkatu during the September test period, Suutarila sensor (middle panel) during October test period and Malmi sensor (right panel) during November test period.

#### 4.2.5 Relative humidity and temperature

The meteorological parameters, RH and temperature, correlated very well between the sensors and the reference instruments. For temperature, all the correlation coefficients  $R^2$  were above 0.99 and the correction factors  $CF_1$  between 0.96 and 1.01 and  $CF_2$  between -0.5 °C and 0.25 °C. The correction factors for temperature are thus not shown in this document. For RH, only the Pakila vara –sensor showed some problems, having correlation coefficient  $R^2$  of 0.83. However, we noticed that during the test periods covering the whole autumn 2017, the reference instruments did not exceed 90 % relative humidity. This suggest that the derivation of correction factors would be at least partly influenced by the uncertainties in the reference instrument, and thus we do not show the RH correction factors in this document.

### 4.3 Precision and accuracy of the Pegasor AQ Urban

Seven Pegasor AQ Urban instruments were flow calibrated prior their testing for precision. The maximum deviation of the flow rates was found to be less than  $\pm 20\%$  excluding the AQ Urban used in Kallio (deviation of 27.7 %) which had been running for more than 3.5 years without service. The long continuous operation most likely accounted for the greater deviation, since the operation histories of the other instruments were shorter (1.9-2.7 years). The precision testing was conducted at the Mäkelänkatu supersite by using the Mäkelänkatu unit as a reference point. At each time period, two AQ Urban units were placed alongside the reference unit (Fig. 4.3.1) and the outputs of these instruments were compared. After the test period, the two units were replaced with another set of AQ Urban instruments. The results of the inter-comparison are shown in Table 1. The coefficients of determination ( $R^2$ ) were very high (0.995-0.999) and the slopes and intercepts indicated a maximum deviation of approximately  $\pm 3\%$  and  $\pm 0.26 \mu\text{m}^2 \text{cm}^{-3}$  across all instrument units. The results show that the Pegasor AQ Urban instruments are very consistent monitors.

The accuracy of the AQ Urban was also assessed at the Mäkelänkatu supersite station. The test period lasted from 4.6.2018 to 27.1.2019 covering approximately half year. Vienna type differential mobility particle analyzer (DMPS, Aalto et al. 2001) with an Airmodus A20 particle counter (Vanhanen et al. 2011) was used as a reference instrument. This instrument measured particle number concentrations from 6 to 800 nm. Scatter plot of LDSA measured with the AQ Urban and calculated from the size distribution of the DMPS is shown in Figure 4.3.2. The coefficient of determination ( $R^2$ ) was 0.89 which appears to be similar to what has been found in previous studies (Kuula et al., 2018;  $R^2 = 0.93$ ). Correction factor of 1.35 ( $\approx 1/0.74$ ) was used for AQ Urban instruments in HAQT project to obtain equivalent LDSA results with DMPS. Considering the results from the precision and accuracy testing, the Pegasor AQ Urban is a stable and accurate instrument for the measurement of particles emitted from local combustion sources.



**Figure 4.3.1.** Co-located precision measurement configuration. The AQ Urban (Mäkelänkatu unit) located in the middle was used as a reference. Photo © HSY / Anssi Julkunen.

**Table 4.3.1.** Precision of AQ Urban units compared to the Mäkelänkatu unit.

Unit	Test start time	Test end time	Test duration (days)	R <sup>2</sup>	Slope	Intercept
Kumpula	29.11.2018 15:00	14.12.2018 9:00	15	0.996	1.0160	-0.0533
Kallio	29.11.2018 15:00	14.12.2018 9:00	15	0.995	0.9689	-0.0887
Itä-Hakkila	19.12.2018 15:00	3.1.2019 9:00	15	0.996	1.0135	-0.0614
Rekola 2	19.12.2018 15:00	3.1.2019 9:00	15	0.997	0.9891	0.0446
Hiekkaharju	11.1.2019 16:00	23.1.2019 13:00	12	0.999	0.9793	-0.2495
Luukki	11.1.2019 16:00	23.1.2019 13:00	12	0.999	1.0100	-0.2555

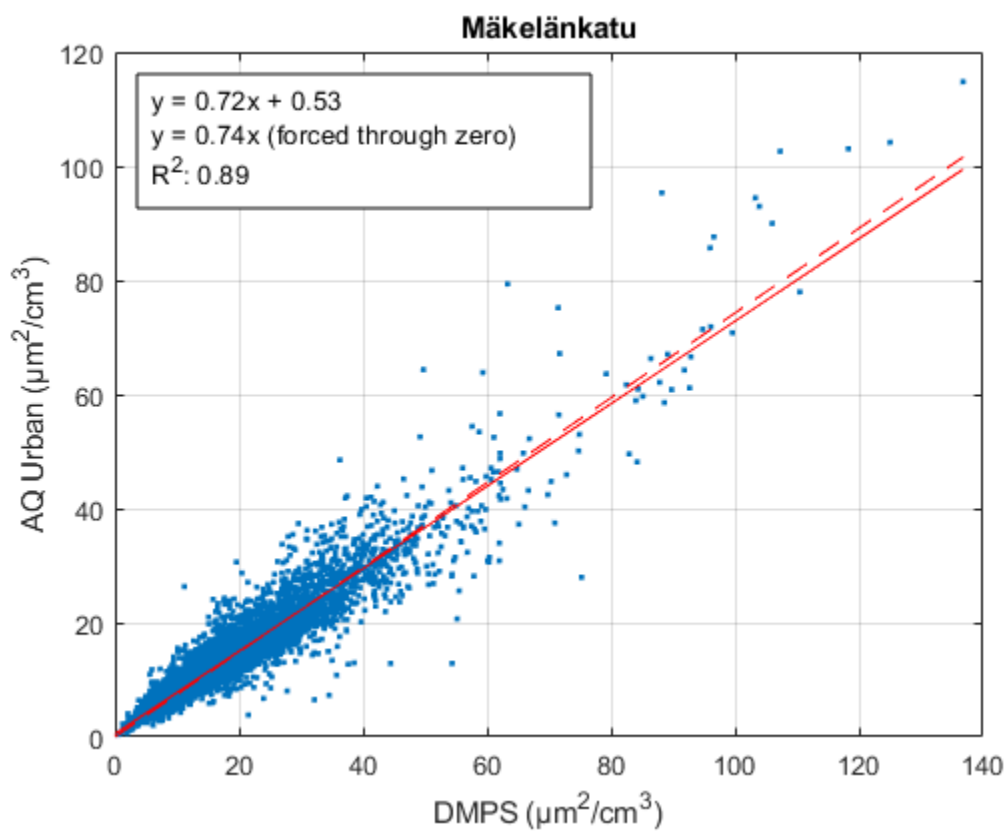


**Figure 4.3.2.** Hourly LDSA concentrations measured with AQ Urban and DMPS in Mäkelänkatu. The measurements were conducted from 4.6.2018 to 27.1.2019 (approximately half year). The dashed red line signifies linear fit forced through zero.

## 5. Conclusions

### 5.1 Laboratory results

The performance of the Vaisala Air Quality Transmitter AQT420 sensor systems (Release 2017) were tested in laboratory conditions against reference methods following the draft document that was being developed and constantly updated by the CEN/TC264/WG42: “Air quality – Performance evaluation of air quality sensors – Part 1: Gaseous pollutants in ambient air”. We wanted to evaluate, if the performance of the selected type of instruments are applicable for air quality measurements fulfilling the data quality objective for indicative measurements according to Air Quality Directive 2008/50/EC.

As a summary, the AQT420 sensor system (2017 Revision) passed part of the requirements for test quantities or performance parameters for Class 1, Class 2 or Class 3 sensor systems; however, not all the requirements set in the draft of the Technical Specification being developed for the performance testing of air quality sensors were met. For some gases and test quantities the parallel sensor systems showed very similar results between each other but in some cases the results of parallel sensor systems differed notably. The most notable requirement exceedances were determined for response times of all the gas components investigated. This is mostly due to the algorithms used for calculating the measurement results of the individual measurement sensors; probably, by improving the algorithms of the AQT420 sensor system it is likely to fit into the required response times and thus also other test quantity requirements. Unfortunately, not all the proposed test quantities could be determined, and consequently, the total measurement uncertainty also could not be calculated.

Additional laboratory tests with the AQT420 sensor (2017 Revision) showed that the AQT420 was able to detect aerosol particles down to 250 nm in size. In the subsequent laboratory tests, we used a prototype optics for the AQT 420 with blue laser (405 nm wavelength). In these tests the lowest detectable particles were 200 nm in diameter. The results showed that perpendicular polarized laser has a five-fold larger scattering cross section compared with parallel polarized laser. This indicated potential in improving the optics of the AQT 420 sensor towards detecting smaller particles.

### 5.2 Atmospheric observations

Based on the side-by-side intercomparison of the aerosol mass measurements in Mäkelänkatu, the AQT 420 sensors (2017 Revision) showed clearly more single peaks than the TEOM 1405 data especially for PM<sub>2.5</sub> measurements. Furthermore, there was considerable large variation between sensor individuals on the response to the particulate mass concentrations.

A comparison study of AQT-420 sensors (2017 Revision) against the reference method for the PM<sub>2.5</sub> and PM<sub>10</sub> size fraction was performed. Following the guidelines, the raw data was corrected against the reference method. Subsequently the data from AQT 420 sensors was within the expanded uncertainty defined by the AQ-directive, (AQD 2008/50/EC, 2008) with PM<sub>10</sub> mass concentrations, but not in PM<sub>2.5</sub> mass concentrations. From the regression analysis it is evident that in case of PM<sub>2.5</sub> measurements, no agreement with the data quality objectives (DQO) according to AQ-directive is achieved for indicative measurements while in case of PM<sub>10</sub> all sensors fulfill the DQO.

The sensor derived gas phase and aerosol mass concentrations were explored in more detail. The results indicated that in case of daily average data the influence of the relative humidity is clearly seen.

This needs to be explored in more detail with extended data sets. Plausible explanation for this behavior is the fact that the AQT 420 mass measurement relies on optical size distribution measurements and the mass is calculated based on this data. The optical measurement is performed without drying the sampled particles. There are two consequences of high humidity to this technology. Firstly, the aerosol particles tend to grow in size due to their hygroscopicity (e.g. Swietlicki et al. 2008). The growth particles are larger and some of the ultra-fine particles can grow to the detectable sizes as well as already detected particles can be associated as larger and therefore contributing to an increase in mass. Secondly, particularly during fog, some of the fog droplets can find their way into the optical detector. As their size is in the micrometer range, they are classified as aerosol mass. The reference method includes sample flow heating evaporating the fog droplets before detection of mass.

The determination of correction factors for the concentrations observed with AQT 420 showed that the sensor response to NO<sub>2</sub> concentrations is good and the corrections with simple linear fit is enough. For CO concentrations, the relative bias between the sensor and the reference instrument was observed to depend on temperature. The positive sensor to reference bias increased for most of the sensors when the temperature moved further from +5 degC to either direction. By introducing an additional temperature correction function, the correlations between sensor and reference instruments were improved. The ozone concentration showed the weakest correlation out of gaseous pollutants between sensors and the reference instrument. The bias of some of the sensors was observed to correlate with temperature, but since these connections were inconsistent between test periods we did not parameterize this dependency

For PM<sub>10</sub> we derived correction factors both for linear and logarithmic concentrations. With linear correction factors the peak concentrations were captured better, whereas with the logarithmic correction the sensor agreed with the reference relatively well in both high and low concentrations, however, showing more absolute discrepancy under high concentrations. Relative humidity was observed to influence the bias in the PM<sub>10</sub> concentrations from most of the sensors. However, as the dependency was non-linear and not consistent between the sensors and test periods, we did not parameterize this dependency. Furthermore, we did not derive correction factors for PM<sub>2.5</sub>, since the correlations were not strong enough to reliably determine such.

Additionally, 7 Pegasor AQ Urban instruments were tested against state-of-the-art instruments in determining lung-deposited surface area of the atmospheric aerosols (LDSA). Linear regression indicated that the slopes and intercepts indicated a maximum deviation of approximately  $\pm 3\%$  and  $\pm 0.26 \mu\text{m}^2 \text{cm}^{-3}$  across all instrument units. The results show that the Pegasor AQ Urban instruments are very consistent monitors. Overall, the Pegasor AQ Urban is a stable and accurate instrument for the measurement of particles emitted from local combustion sources.

## References

- Aalto, P., Hämeri, K., Becker, E., Weber, R., Salm, J., Mäkelä, J. M., Kulmala, M. (2001). Physical characterization of aerosol particles during nucleation events. *Tellus B*, 53, 344-358.
- AQD 2008/50/EC: Directive of the European Parliament and of the Council of 21 May 2008 on ambient air quality and cleaner air for Europe.
- Beijk R., Mooibroek D., van de Kasstele J., Hoogerbrugge R., 2008. PM10: Equivalence study 2006 Demonstration of equivalence for the automatic PM10 measurements in the Dutch National Air Quality Monitoring Network. A technical background report Report, RIVM 680708002/2008.
- von Bismarck-Osten, C., Birmili, W., Ketzler, M., Massling, A., Petäjä, T. and Weber, S. (2013) Characterization of parameters influencing the spatio-temporal variability of urban particle number size distributions in four European cities, *Atmos. Environ.* 77, 415-429.
- EN 12341: 2014. Air Quality – Standard gravimetric measurement method for the determination of the PM10 or PM2.5 mass concentration of suspended particulate matter.
- GDE, 2010, Guide to the Demonstration of Equivalence of Ambient Air Monitoring Methods. <http://ec.europa.eu/environment/air/quality/legislation/pdf/equivalence.pdf>.
- Häkkinen, E. (2017) Aerosolimittalaitteiden kalibroitimenetelmän kehitys (Development of Calibration Method for Aerosol Instruments), BSc. Thesis, Metropolia AMK, Helsinki, 38 pages.
- Johansson, L., Epitropou, V., Karatzas, K., Karppinen, A., Wanner, L., Vrochidis, S., Bassoukos, A., Kukkonen, J. and Kompatsiaris I. (2015) Fusion of meteorological and air quality data extracted from the web for personalized environmental information services. *Environ. Model. Software*, 64, 143-155.
- Järvinen, A. (2018) Improving sensitivity and reliability of optical PM2.5 measurement, Master's thesis in technology, University of Turku, 136 pages.
- Järvinen, A., Kuuluvainen, H., Niemi, J.V., Saari, S., Dal Maso, M., Pirjola, L., Hillamo, R., Janka, K., Keskinen, J. and Rönkkö, T. (2015). Monitoring urban air quality with a diffusion charger based electrical particle sensor. *Urban Clim.* 14: 441–456.
- Kukkonen, J.K., Karl, M.K., Keuken, M.P., Denier van der Gon, H.A.C., Denby, B.R., Singh, V., Douros, J., Manders, A., Samaras, Z., Moussiopoulos, N., Jonkers, S., Aarnio, M., Karppinen, A., Kangas, L., Lützenkirchen, S., Petäjä, T., Vouitsis, I. and Sokhi, R.S. (2016) Modelling the dispersion of particle numbers in five European cities, *Geosci. Model. Dev.* 9, 451-478.
- Kuula, J., Kuuluvainen, H., Rönkkö, T., Niemi, J.V., Saukko, E., Portin, H., Aurela, M., Saarikoski, S., Rostedt, A., Hillamo, R. And Timonen, H. (2018) Applicability of optical and diffusion charging-based particulate matter sensors to urban air quality measurements, *Aerosol Air Qual. Res.* 19, 1024-1039.
- Morawska, L., Thai, P.K., Liu, X., Asumadu-Sakyi, A., Ayoko, G., Bartonova, A., Bedini, A., Chai, F., Christensen, B., Dunbabin, M., Gao, J., Hagler, G.S.W., Jayaratne, R., Kumar, P., Lau, A.K.H., Louie, P.K.K., Mazaheri, M., Ning, Z., Motta, N., Mullins, B., Rahman, M.M., Ristovski, Z., Shafiee, M., Tjondronegoro, D., Westerdahl, D. and Williams, R. (2018) Applications of low-cost sensing technologies for air quality monitoring and exposure assessment: How far have they gone? *Environ. Int.* 116, 286-299.
- Mordas, G., Manninen, H.E., Petäjä, T., Aalto, P.P., Hämeri, K. and Kulmala, M. (2008) On operation of the Ultra-fine Water-based CPC TSI 3786 and comparison with other TSI models (TSI3776, TSI3772, TSI3025, TSI3010, TSI3007) *Aerosol Sci. Technol.*, 42, pp. 152-158.

de Nazelle, A., Seto, E., Donaire-Gonzalez, D., Mendez, M., Matamala, J., Jieuwenhuijsen, M.J., Jerrett, M. (2013) Improving estimates of air pollution exposure through ubiquitous sensing technologies, *Environ. Poll.* 176, 92-99.

Park, Y.M. and Kwan, M.-P. (2017) Individual exposure estimates may be erroneous when spatiotemporal variability of air pollution and human mobility are ignored, *Health & Place*, 43, 85-94.

Rostedt, A., Arffman, A., Janka, K., Yli-Ojanperä, J. and Keskinen, J. (2014). Characterization and response model of the PPS-M aerosol sensor. *Aerosol Sci. Technol.* 48: 1022–1030.

Swietlicki, E., Hansson, H.-C., Hämeri, K., Svenningsson, B., Massling, A., McFiggans, G., McMurry, P.H., Petäjä, T., Tunved, P., Gysel, M., Topping, D., Weingartner, E., Baltensperger, U., Rissler, J., Wiedensohler, A. and Kulmala, M. (2008) Hygroscopic properties of sub-micrometer atmospheric aerosol particles measured with H-TDMA instruments in various environments - a review. *Tellus B* 60, pp. 432-469 doi: 10.1111/j.1600-0889.2008.00350.x.

Yliojanperä, J., Mäkelä, J.M., Marjamäki, M., Rostedt, A. and Keskinen, J. (2010) Towards traceable particle number concentration standard: Single charged aerosol reference (SCAR), *J. Aerosol Sci.* 41, 719-728.

Vanhanen, J., Mikkilä, J., Lehtipalo, K., Sipilä, M., Manninen, H.E., Siivola, E., Petäjä, T. and Kulmala, M. (2011) Particle size magnifier for nano-CN Detection *Aerosol Sci. Technol.*, 45, pp. 533-542.

Waldén, J., Vestenius M. (2018) Verification of PM-analyzers for PM<sub>10</sub> and PM<sub>2.5</sub> with the PM reference method. Finnish Meteorological Institute, Reports 2018:2, 64 pp., Helsinki.

Waldén, J., Waldén, T., Laurila, S., Hakola, H. (2017) Demonstration of the equivalence of PM<sub>2.5</sub> and PM<sub>10</sub> measurement methods in Kuopio 2014-2015. Finnish Meteorological Institute, Reports 2017:1, 134 pp., Helsinki.

Winkmayr, W., Reischl, G.P., Lindner, A.O. and Berner, A. (1991) A new electromobility spectrometer for the measurement of aerosol size distributions in the size range from 1 to 1000 nm, *J. Aerosol Sci.* 22, 289-296.

Zhao, S., Ye, Y., Yin, D., Qin, D., He, J. and Dong, L. (2018) Spatial patterns and temporal variations of six criteria air pollutants during 2015 to 2017 in the city clusters of Sichuan Basin, China, *Sci. Tot. Environ.* 624, 540-557.